

Accepted Manuscript

# *Journal of the Geological Society*

## Clumped isotope evidence for episodic, rapid flow of fluids in a mineralized fault system in the Peak District, UK

Paul Frederick Dennis, Daniel J Myhill, Alina D Marca & Ruth Kirk

DOI: <https://doi.org/10.1144/jgs2016-117>

Received 7 September 2016

Revised 4 October 2018

Accepted 19 October 2018

© 2018 The Author(s). Published by The Geological Society of London. All rights reserved. For permissions: <http://www.geolsoc.org.uk/permissions>. Publishing disclaimer: [www.geolsoc.org.uk/pub\\_ethics](http://www.geolsoc.org.uk/pub_ethics)

Supplementary material at <https://dx.doi.org/10.6084/m9.figshare.3808329.v9>

To cite this article, please follow the guidance at [http://www.geolsoc.org.uk/onlinefirst#cit\\_journal](http://www.geolsoc.org.uk/onlinefirst#cit_journal)

### **Manuscript version: Accepted Manuscript**

This is a PDF of an unedited manuscript that has been accepted for publication. The manuscript will undergo copyediting, typesetting and correction before it is published in its final form. Please note that during the production process errors may be discovered which could affect the content, and all legal disclaimers that apply to the journal pertain.

Although reasonable efforts have been made to obtain all necessary permissions from third parties to include their copyrighted content within this article, their full citation and copyright line may not be present in this Accepted Manuscript version. Before using any content from this article, please refer to the Version of Record once published for full citation and copyright details, as permissions may be required.

# Clumped isotope evidence for episodic, rapid flow of fluids in a mineralized fault system in the Peak District, UK

Paul F. Dennis<sup>1\*</sup>, Daniel J. Myhill<sup>2</sup>, Ruth Kirk<sup>1</sup> and Alina Marca<sup>1</sup>

<sup>1</sup>Stable Isotope Laboratory, School of Environmental Sciences, University of East Anglia, Norwich, NR4 7TJ, UK.

<sup>2</sup>A.F. Howland Associates, 38, Newmarket Road, Norwich, NR4 6UF, UK

\*Corresponding author (e-mail: [p.dennis@uea.ac.uk](mailto:p.dennis@uea.ac.uk))

## Abstract

*We have used clumped isotope thermometry to study a fault-hosted hydrothermal calcite vein associated with the Mississippi Valley Type (MVT) mineralization on the Derbyshire Platform in the southern Pennines, UK. This is the first published data set obtained using a new mass spectrometer, MIRA, optimized for clumped isotope analysis and an associated clumped isotope-temperature calibration. We analysed multiple generations of vein growth at high spatial resolution in two transects across the vein. The vein grew episodically at temperatures between 40° and 100°C. We interpret each episode of growth as being associated with an increasing flux of formation waters from deep sedimentary basins next to the mineralized platform and an accompanying increase in the precipitation temperatures. Heat is conserved in the fluid as it ascends along the fault surface and, thus, flow must have been fast and restricted to short-lived pulses. The flux could have been driven by high pore pressures associated with rapid sedimentation, hydrocarbon generation and diagenesis in the basal facies of the Visean Bowland-Hodder group. Natural hydraulic fracturing of shale units and failure of capillary seals, possibly triggered by uplift, allowed the release of fluids into aquifers within the sediment pile. The transmission of high pore fluid pressures from the shales to the fault zone, aided by the compressibility of the gas phase in two-phase pore fluids, may have resulted in fault rupture, accompanied by enhanced fracture permeability and rapid fluid flow. Vein growth ceased as pore pressures dissipated. Such behaviour is closely related to a seismic valve type model for mineralization. -end abstract*

**Supplementary Information:** Dennis, Paul; Myhill, Daniel; Kirk, R; Marca, Alina (2016): Clumped isotope evidence for episodic, rapid flow of fluids in a mineralized fault system in the Peak District, UK - supplementary information.

<https://dx.doi.org/10.6084/m9.figshare.3808329.v9>

There is abundant evidence that pore fluids and fracture processes in the upper crust are physically and chemically coupled (Hubbert & Rubey 1959; Frank 1965; Nur 1973; Sibson 1981). Increases in

pore fluid pressure, for example due to fluid injection, can lead to rupture and an increase in seismic activity. This is readily explained by the Navier-Coulomb criteria for brittle failure and the decrease in effective stress that results from the elevated pore fluid pressure (Price 1966; Sibson 1981).

Conversely, the changes in groundwater levels and the surface effusions of warm water that sometimes occur along fault traces following earthquakes show that failure can also have a profound effect on fluid flow, heat and mass transport (Nur 1974; Sibson *et al.*; 1975, Sibson 1981). The flow is interpreted to result from either seismic pumping due to a dilatancy-diffusion type process or a seismic valve mechanism in which fault rupture leads to leakage of an over-pressured aquifer or reservoir of fluid (Nur 1972; Sibson 1981).

Direct evidence for episodic and rapid flow of fluids associated with fracture and faulting in the geological record is more equivocal. The presence of banded hydrothermal mineralization of varying degrees of complexity in exhumed fault systems is taken as evidence of pulsed fluid flow driven by seismic activity. Failure results in brecciation of earlier generations of veins and the opening of large dilation voids that are then cemented by mineral precipitation from upwelling fluids (Wright *et al.* 2009). Observations of epithermal mineralization associated with dilation jogs between en-echelon fault segments suggests that in this structural setting fluid flow is rapid and accompanied by pressure fluctuations which trigger high level boiling, or effervescence of hydrothermal fluids. This promotes the precipitation of common gangue quartz and calcite as well as metalliferous minerals of economic importance (Sibson 1975; Sibson 1987; Henley & Berger 2000). In other geologic settings, however, the extent to which mineral precipitation in veins is contemporaneous with and directly coupled to failure is still open to question.

One characteristic of systems with episodic pulsing of hot fluids is the development of a thermal anomaly along the high permeability paths in which the flow is focused. An example is the perturbation of the temperature field observed in the Mississippi Valley Type (MVT) mineralization districts that lie on the margins of major Palaeozoic sediment basins in the continental USA (Sangster *et al.* 1994). Similar temperature anomalies have been reported for other sedimentary basins, for example, to the south east of the Massif Central in France (Charef & Sheppard 1988). The anomaly is seen as a difference between the temperature of precipitation of hydrothermal minerals and that of the host rock at the time and depth of burial that the mineralization took place. Using simple thermal modeling Cathles and co-workers show that the temperature difference is due to heat advection associated with the episodic, rapid release of hot fluids from deeper regions of the basins (Cathles & Smith 1983; Cathles & Adams 2005). They suggest that the fluids originate from overpressured formation water in the compacting sedimentary basins. Importantly, the fluid velocities required to sustain the thermal anomaly are more than 1000 times greater than could be produced by the steady subsidence, compaction and dewatering of the basins (Cathles & Smith 1983). This suggests to us that the pulses result from a coupling between the pore fluid pressure and rock failure. When pore fluid pressures approach lithostatic either hydraulic fracturing or shear failure occurs with the development of dilation jogs along fault surfaces. This allows rapid dewatering of shales within the sediment pile. In the basins studied by Cathles the fluid is channeled into high permeability aquifers from where it rapidly flows outwards towards the basin margins. This model is at direct variance with those that invoke gravity driven basin-wide migration of fluids from a high-altitude recharge area towards discharge regions on the other side of the basin (e.g. Garven & Freeze 1984; Garven *et al.* 1999).

Mineralization with MVT affinities occurs within the Peak District area of the southern Pennines in the UK. Here strata bound deposits (flats) of dominantly Pb-Zn and fluorite mineralization are closely associated with near vertical veins (rakes and scrins) that lie along strike-slip fault surfaces and fractures of Variscan age (Ford & Worley 2016; Quirk 1993). The mineralization is restricted to lower

Carboniferous shelf carbonates that lie along the margins of half-graben basins filled with lower and upper Carboniferous silici-clastic sediments. It is widely held that the mineralization results from basin scale migration of sedimentary formation waters (Ixer & Vaughan 1993). However, the driving force for, flow paths and rates of fluid migration are poorly constrained. Opinion ranges from slow gravity driven flow as a result of tectonic uplift associated with the Variscan orogeny (Quirk 1991) to a seismic valve type process with rapid dewatering of the over-pressured basin fill triggered by fault activity (Hollis & Walkden 2002; Frazer *et al.* 2014). Evidence for a thermal anomaly associated with advection of fluids is inconclusive. Fluid inclusion homogenization temperatures for gangue fluorite and calcite associated with the mineralization span a wide range from 70° to >240°C (Atkinson 1983; Hollis & Walkden 2002; Kendrick *et al.* 2002). Mineralization is thought to have occurred at depths between 1 and 2km (Colman *et al.* 1989). Thus, assuming a geothermal gradient of 30° to 50°C km<sup>-1</sup>, the fluid inclusion homogenization temperatures are at, or greater than the maximum expected host rock temperature at the time of mineralization. This suggests that fluid movement was rapid and therefore, unlikely to be associated with slow, gravity driven flow, or a gradual dewatering of the basin fill. There are questions, however, as to the reliability of some of the reported temperatures that are derived from fluid inclusion analysis with little agreement among researchers as to the temperature associated with different paragenetic phases.

To help us better understand the possible coupling between faulting, fluid flow and mineralization in the Peak District we have used clumped isotope thermometry to determine the temperature at which a Variscan hydrothermal calcite vein precipitated. Clumped isotope thermometry is based on the ordering of rare, heavy isotopes of carbon (<sup>13</sup>C) and oxygen (<sup>18</sup>O) in the carbonate lattice. As a result of the greater stability of the <sup>13</sup>C - <sup>18</sup>O bond compared to bonds involving either no, or a single isotopic substitution there is a tendency for the heavy isotopes to order, or clump together. The degree of ordering is an inverse function of temperature. As temperature increases, the isotopes tend towards a more random or stochastic distribution (Eiler 2007). Measurement of the degree of ordering allows us to estimate the temperature at which the distribution of isotopes in the calcite structure are locked in (Ghosh *et al.* 2006). For carbonate minerals precipitating from hydrothermal fluids at mild temperatures (<100-120°C) and suffering no subsequent period of heating such as a metamorphic event that will reset the isotope ordering through solid state diffusion or recrystallisation mechanisms this temperature is very close to or equal to the temperature of precipitation (e.g. see Passey & Henkes, 2012, Huntington & Lechler, 2015; Stolper & Eiler, 2015). A key advantage of the method is that the temperature estimate is based on the distribution of carbon and oxygen isotopes within a single phase and not on the partitioning of oxygen isotopes between calcite and its parent fluid as in the conventional oxygen isotope geothermometer. Thus, determination of the mineral precipitation temperature is decoupled from knowledge of the parent fluid oxygen isotope composition. Combining the clumped isotope temperature (T( $\Delta_{47}$ )) with the bulk oxygen isotope composition of the carbonate represented by its  $\delta^{18}\text{O}$  value we can constrain the isotopic composition of the parent fluid.

Recently, several studies have demonstrated the use of clumped isotopes to help understand the temperature, isotopic composition and fluxes of fluids associated with faulting and fractures in the upper crust (Swanson *et al.* 2012; Bergman *et al.* 2013; Huntington & Lechler, 2015; Luetkemeyer *et al.*, 2016; Hodson *et al.*, 2016; Siman-Tov *et al.*, 2016; Cruset *et al.*, 2016).

## Geological setting of the Variscan faults and vein fill

The geographic location and regional geology of the Peak District area of the southern Pennines is summarized in Figures 1 and 2. During the mid-Devonian to the end of the lower Carboniferous Britain was subject to a general north-south back arc stretching as a result of subduction of the Rheic

ocean to the south of the Variscan front. Extension was accommodated by the development of a series of graben and half graben deep water basins bounded by normal growth faults and separated by foot wall topographic highs. In the Peak District the main basins are the Edale Gulf, the Goyt Trough and the Widmerpool Gulf. Visean shallow water platform and ramp carbonates accumulated on the topographic highs of the Derbyshire platform whilst deep water facies limestones and shales of the Bowland-Hodder group were deposited in the basins (see Fig. 1). The end of the Visean is marked by the cessation of extension and carbonate sedimentation on the platform, followed by the onset of thermal subsidence. Sedimentation accompanying this regional subsidence included a blanket of Namurian shales and later Westphalian river and deltaic sandstone facies. The total thickness of post-Visean sediment accumulation is between 1 and 2 km.

A regional inversion during the Variscan orogeny resulted in significant uplift and exhumation with removal of the Upper Carboniferous cover. During this period, earlier extensional faults were reactivated with both strike-slip and reverse components of movement. Whilst there is little field evidence for a subsequent Mesozoic and Cenozoic cover of the platform, apatite fission track analysis suggests that a significant late-Palaeozoic and Mesozoic cover up to 1.4km thick may have existed and was subsequently removed during Cenozoic uplift associated with the Alpine orogeny (Hillis *et al.* 2008).

The seismic profile and section shown in Figure 2 is taken across the north margin of the platform. The Castleton and associated faults that form the southern margin of the Edale Gulf are clear in this section. The lack of internal deformation in the Edale Basin sediments is also evident and the present basin topography is essentially unchanged from the end of the Visean. Whilst there is no extant thermal modelling of the Edale Basin recent work has been done on the Widmerpool Gulf to the south of the Derbyshire Platform. This is part of ongoing assessment of the shale gas resource potential of the Bowland-Hodder unit. For the Widmerpool Gulf a maximum burial depth of 3.6km for the base of the Bowland-Hodder shale unit is estimated to have been reached at the end of the Carboniferous period. A high modelled heat flow in excess of  $70 \mu\text{W m}^{-2}$  resulted in a geothermal gradient of close to  $50^\circ\text{C km}^{-1}$ . Maximum temperatures at the base of the basin are inferred to be close to  $200^\circ\text{C}$  (Andrews, 2013). Vitrinite reflectance (VR) data suggest somewhat lower maximum temperatures of between  $110^\circ$  and  $140^\circ\text{C}$  (Andrews, 2013). The maximum burial depth for the platform is somewhere between 1 and 2 km with lower maximum temperatures. Apatite fission track analysis and VR data for shales from the upper Carboniferous on the platform suggests maximum temperatures of  $60\text{-}70^\circ\text{C}$  (Green, 2005).

Dirtlow Rake [SK148 818] is a major WSW-ENE trending strike slip fault lying just to the south of Castleton, Figure 1. It is associated with the Castleton fault system that bounds the Edale Gulf to the north. The fault is exposed in a series of old surface workings where excavations up to 10 metres wide and several 10's of metres long have been made for the commercial extraction of galena and sphalerite (Barnatt 2002). These old pits can be traced along the length of the fault for a distance of more than 10km. Where exposed individual slip planes are characterized by sub-horizontal mullion structures and well-developed slickensides. Within the fault zone and adjacent rock mass there is a pervasive mesoscale fracturing with variable fracture orientations and widths ranging from sub-mm through to several cms. The fault shows an extensive development of a complex vein fill dominated by calcite with variable amounts of barite, fluorite, galena and sphalerite. The calcite occurs as large (several cm long), elongate, syntaxial crystals. The growth form is often sparry with rhombohedral and scalenohedral terminations. Intimate intergrowth of galena, calcite and barite suggests that the veins are equivalent to the zone 4 calcite of the mineral paragenesis described by Hollis and Walkden (2002).

The vein used for this study (DLR7) was collected from a large excavation pit [SK14880 81805]. The block of material was not in-situ but lying adjacent to a similar section of vein growing syntaxially from the fault wall. Individual crystals of calcite are up to 10cm long x 1cm wide, Fig. 3. They grow parallel to the c-axes. In hand specimens and thin sections there is evidence of zoned crystal growth marked by colour variations, crystallographically controlled planes of separation and surfaces with high inclusion densities, Figure 3. We could not identify any areas of the hand specimens or thin sections in which there is evidence of post precipitation alteration, including corrosion and recrystallisation that might be suggestive of later surface resetting of the isotopic signatures as a result of dissolution and reprecipitation.

## Methods

### Sample preparation and mass spectrometry

We slabbed a large block of the Dirlow Rake vein and, using a Dremel drill and dental bit, sampled the calcite at 5mm intervals along the growth axis. We took samples from two separate transects separated laterally by approximately 30cm. At each sampling point we drilled approximately 20mg of calcite powder in the form of a small trench (1mm wide x 1mm deep x 10mm long) oriented perpendicular to the growth direction (see the supplementary information). So as to minimize any frictional heating of the sample we avoided using any undue pressure during the drilling.

To produce the analyte CO<sub>2</sub> we reacted *in vacuo* in pear shaped reaction vessels sealed with a Louwers-Hapert vacutap, 6-8mg of sample powder with 102% ortho-phosphoric acid for a period of 12 hours. The reaction temperature was closely controlled ( $\pm 0.1^\circ\text{C}$ ) at  $25^\circ\text{C}$  by placing the reaction vessels in a thermostatically controlled water bath. The evolved CO<sub>2</sub> was dried, collected by cryo-distillation into a calibrated volume manometer to check reaction yields and then stripped of contaminants before collection in a glass gas tube sealed with a Louwers-Hapert glass vacutap. The drying stage involves freezing the CO<sub>2</sub> into a glass spiral trap at liquid nitrogen temperatures before sublimation at  $-120^\circ\text{C}$  and passing the gas through a second trap at  $-120^\circ\text{C}$  whilst freezing with liquid nitrogen into the manometer. We stripped any potential hydrocarbon and chlorocarbon contaminants from the CO<sub>2</sub> by cryo-distillation into the gas tube via a 20cm x 4mm i.d. glass tube packed with porapak Q ion exchange resin and held at a temperature of  $-20^\circ\text{C}$ .

The sample gases were analysed for their isotope values,  $\delta^{45}$  -  $\delta^{49}$  on the UEA MIRA dual-inlet isotope ratio mass spectrometer. The design, construction and performance of this mass spectrometer is described fully in the supplementary information. All analyses are made at a major beam ( $m/z = 44$ ) intensity of  $7.5 \times 10^{-8}\text{A}$  with simultaneous data acquisition for each cardinal mass of the CO<sub>2</sub> molecule ( $m/z = 44 - 49$ ). Each measurement consists of 4 acquisitions, each of 20 reference-sample gas pairs. Before analysis and between each acquisition the sample and reference gas volumes and signal strengths are balanced to within 1% of each other. After switching of the changeover valve, sample, or reference cycles consist of a 10s dead time followed by a 20s integration period. The total measurement time for each analysis, including sample and reference gas balancing is approximately 90 minutes. This results in an integration time of 1600s each for the sample and reference gas. Internal precisions ( $\pm 1\sigma$ ) for  $\delta^{45}$  and  $\delta^{46}$  are better than 0.001‰, for  $\delta^{47}$  better than 0.008‰, for  $\delta^{48}$  better than 0.03‰ and for  $\delta^{49}$  better than 10‰.

The mass spectrometer working reference gas (wrg) is produced by reaction of BDH marble chips with 85% ortho-phosphoric acid and subsequently equilibrated with laboratory water at  $20^\circ\text{C}$  for a

period of 1 month. This is to ensure (i) that the bulk isotopic composition of the reference gas,  $\delta^{13}\text{C}$  and  $\delta^{18}\text{O}$ , are close to corresponding values for the sample gas and (ii) the  $\Delta_{47}$  value of the reference gas is in equilibrium at the laboratory temperature. An advantage of using a mass spectrometer wrg that is close in bulk isotope composition to sample gases is that determination of accurate  $\Delta_{47}$ ,  $\Delta_{48}$  and  $\Delta_{49}$  values is insensitive to the algorithm used to correct for  $^{17}\text{O}$  contributions to the  $\delta^{45}$  and  $\delta^{46}$  values and thus determination of  $\delta^{13}\text{C}$  and  $\delta^{18}\text{O}$  values. In addition, the corrected values of  $\delta^{13}\text{C}$  and  $\delta^{18}\text{O}$  are also independent of the precise values used for the absolute ratios ( $R_{13}^{\text{VPDB}}$ ,  $R_{17}^{\text{VSMOW}}$  and  $R_{18}^{\text{VSMOW}}$ ) of the standards VPDB and VSMOW (e.g. see Daeron *et al.* (2016); Schauer *et al.*, 2016). The composition of the reference gas is:  $\delta^{13}\text{C} = 2.007\text{‰}_{\text{VPDB}}$ ,  $\delta^{18}\text{O} = 34.899\text{‰}_{\text{VSMOW}}$  and  $\Delta_{47} = 0.94\text{‰}$ . To ensure a robust calibration of scale compression and transfer function between the local reference frame for  $\Delta_{47}$  and the absolute reference frame (ARF) both  $1000^\circ\text{C}$  heated and  $20^\circ\text{C}$  water equilibrated reference gas samples are measured on a daily basis (Dennis *et al.* 2011). Data quality and long term stability of measured values is monitored by measurement of two laboratory standards that bracket the range of  $\Delta_{47}$  values for samples in this study: UEACMST ( $\Delta_{47} = 0.384 \pm 0.013\text{‰}$ ,  $n=47$ ) and UEAHTC ( $\Delta_{47} = 0.562 \pm 0.014\text{‰}$ ,  $n=14$ ). Based on the analyses of standards our best estimate of the external precision for individual sample analyses is  $\pm 0.014\text{‰}$ .

The MIRA response is neutral with respect to the calculated  $\Delta_{47}$  and  $\Delta_{48}$  values of samples as a function of their bulk isotopic composition as represented by their  $\delta^{47}$  and  $\delta^{48}$  values (c.f. Huntington *et al.* 2009). In spite of this we regularly check for linearity by measurement of  $1000^\circ\text{C}$  heated cylinder  $\text{CO}_2$  (BOC) that is depleted in  $\delta^{47}$  with respect to the reference gas by approximately 65‰.

## Data handling and calculation of $\Delta$ values

The clumped isotope  $\Delta_i$  value of a sample is defined as:

$$D_i = \left( \frac{R_i}{R_i^*} - 1 \right) \cdot 1000 \quad (1)$$

where  $R_i$  is the measured ratio of isotopologue  $i$  to the non-isotopically substituted isotopologue and  $R_i^*$  is the expected ratio assuming a stochastic distribution of all isotopes over all possible sites in the lattice (Wang *et al.* 2004). For  $\text{CO}_2$  we are largely concerned with the multiply substituted isotopologue  $^{13}\text{C}^{18}\text{O}^{16}\text{O}$  ( $i = 47$ ). In addition, we also determine  $\Delta$  values for  $^{13}\text{C}^{18}\text{O}^{17}\text{O}$  ( $i = 48$ ) and  $^{13}\text{C}^{18}\text{O}^{18}\text{O}$  ( $i = 49$ ).

$\Delta_{47}$  values were calculated using the established algorithms outlined by Huntington *et al.* (2009) with the exception of using the updated  $^{17}\text{O}$  correction protocol and values proposed by Daeron *et al.* (2016).

The ratios  $R_i$  and  $R_i^*$  are determined from the measured  $\delta^i$  values of the sample  $\text{CO}_2$  measured with respect to the mass spectrometer working reference gas. For  $R^{47}$ :

$$R_{47}^{\text{sam}} = \left( \frac{d_{\text{sam-wrg}}^{47}}{1000} - 1 \right) \cdot R_{47}^{\text{wrg}} \quad (2)$$

□

where  $R_{47}^{wrg}$  is the 47/44 ratio of the working reference gas (wrg) and is determined as:

$$R_{47}^{wrg} = 2 \times R_{13}^{wrg} \times R_{18}^{wrg} + 2 \times R_{18}^{wrg} \times R_{17}^{wrg} + R_{13}^{wrg} \times (R_{17}^{wrg})^2 \quad (3)$$

Note that implicit in this treatment is an assumption that the mass spectrometer working reference gas has a stochastic distribution of isotopes. It is self-evident that this is incorrect since the working reference gas has been equilibrated with water at the laboratory temperature. However, since the  $\Delta$  values are  $<1\%$  we can make this assumption and carry out a later linear transformation of the data onto an absolute reference frame (ARF) to take account of the actual reference gas  $R_{47}$  value without introducing any significant errors (see below).

In equation (3), the ratios,  $R_{13}^{wrg}$  and  $R_{18}^{wrg}$  are determined from the  $\delta^{13}\text{C}_{\text{wrg-VPDB}}$  and  $\delta^{18}\text{O}_{\text{wrg-VSMOW}}$  values of the working reference gas:

$$R_{13}^{wrg} = \left( \frac{d_{\text{wrg-VPDB}}^{13}}{1000} + 1 \right) \cdot R_{13}^{\text{VPDB}} \quad (4)$$

and similar equations for  $R_{18}$ .  $R_{17}^{wrg}$  is determined using:

$$R_{17}^{wrg} = k \times (R_{18}^{wrg})^l \quad (5)$$

where  $k$  is given by:

$$k = R_{17}^{\text{VSMOW}} \times (R_{18}^{\text{VSMOW}})^{-l} \quad (6)$$

We have used  $\lambda = 0.528$ , as recommended by Brand *et al.* (2010). The reference gas ratios are  $R_{13}^{\text{VPDB}} = 0.01118$ ,  $R_{17}^{\text{VSMOW}} = 0.00038475$  and  $R_{18}^{\text{VSMOW}} = 0.00208835$  (Daeron *et al.*, 2016).

The sample ratios  $R_{45}^{\text{sam}}$ ,  $R_{46}^{\text{sam}}$ ,  $R_{48}^{\text{sam}}$  and  $R_{49}^{\text{sam}}$  are calculated in a similar fashion to  $R_{47}^{\text{sam}}$  given above in eqn. 2 (see the supplementary information).

We have used the Santrock algorithm (Santrock *et al.*, 1985) to determine  $R_{18}^{\text{sam}}$  from the measured  $R_{45}^{\text{sam}}$  and  $R_{46}^{\text{sam}}$  values (with  $\lambda = 0.528$  and  $k = 0.0102246$  (eqn. (6)).  $R_{17}^{\text{sam}}$  is determined using an equation of the form of eqn. (5). Finally,  $R_{13}^{\text{sam}}$  is calculated as:

$$R_{13}^{sam} = R_{45}^{sam} - 2 \times R_{17}^{sam} \quad (7)$$

Bulk isotope  $\delta^{13}\text{C}_{VPDB}$  and  $\delta^{18}\text{O}_{VSMOW}$  values are calculated using:

$$\delta^{13}\text{C}_{VPDB} = \left( \frac{R_{13}^{sam}}{R_{13}^{VPDB}} - 1 \right) \cdot 1000 \quad (8)$$

and;

$$\delta^{18}\text{O}_{VSMOW} = \left( \frac{R_{18}^{sam}}{R_{18}^{VSMOW}} - 1 \right) \cdot 1000 \quad (9)$$

The expected stochastic ratios,  $R_i^*$ , for the multiply substituted isotopologues in the sample gas are determined, using the  $R_{47}^*$  ratio as an example:

$$R_{47}^* = 2 \times R_{13}^{sam} \times R_{18}^{sam} + 2 \times R_{18}^{sam} \times R_{17}^{sam} + R_{13}^{sam} \times (R_{17}^{sam})^2 \quad (10)$$

Substitution of  $R_{47}^{sam}$  (equation (2)) and  $R_{47}^*$  (equation (10)) into equation (1) allows determination of  $\Delta_{47}$ . Evaluation of  $\Delta_{48}$  and  $\Delta_{49}$  follows the same steps as above. The complete data reduction algorithm and its implementation in a Mathematica program for data obtained on the MIRA mass spectrometer is included in the supplementary information.

Using the heated and water equilibrated gas standards we determine a transfer function for  $\Delta_{47}$  between the local reference frame (LRF), that is for measurements made with respect to the mass spectrometer working reference gas and the absolute reference frame (ARF) (Dennis *et al.* 2011). Data for  $\Delta_{48}$  are reported on the local reference frame.

## Temperature estimation using $\Delta_{47}$

Using the clumped isotope composition of carbonate minerals as a geothermometer is a relatively new and still developing technique. Critical to its successful application is a robust calibration between  $\Delta_{47}$  and temperature. At present there exist many different calibrations (e.g. Ghosh *et al.* 2006; Dennis & Schrag 2010; Henkes *et al.* 2013; Petrizzo *et al.* 2014; Tang *et al.* 2014; Wacker *et al.* 2014; Kirk, 2016; Kelson *et al.* 2017) with a range in both the temperature sensitivity and offset of the different

studies. Differences between calibrations partially depends on the absolute values of reference gas isotope ratios and form of the  $^{17}\text{O}$  correction algorithm used during data processing (Daeron *et al.* 2016, Kelson *et al.*, 2017). Recent attempts to standardize data correction using the ratio values and parameters suggested by Brand *et al.* (2017) indicate that much of the discrepancy between studies is eliminated. Not-with-standing this there are still differences between different calibration studies This indicates that there still exist factors that may be dependent on the exact analytical protocol adopted by different laboratories that include reaction temperature, static *versus* dynamic reaction and gas collection, drying temperatures and whether a static porapak or GC based porapak trap is used to remove potential contaminant species.

For this study we have used the temperature calibration determined at UEA using biogenic carbonates (bivalves and foraminifera) and travertine samples collected from sites with well characterized temperatures (Kirk, 2016) and were prepared under similar conditions to the samples from this study:

$$D_{47} = \frac{3.890 \times 10^4}{T^2} + 0.2139 \quad (11)$$

where  $T$  is absolute temperature. Details of the temperature calibration are given in Kirk (2016) and the supplementary information. The calibration has been made over a restricted temperature range (0-56°C). For the most part this range is below the temperature of the samples reported in this study. We have confidence, however, that the calibration can be extrapolated to higher temperatures. The  $\Delta_{47}$  value (+0.27) we measure for a Carrara marble sample that had been crushed and experimentally recrystallized at 600°C and 1000MPa in a solid media apparatus before rapidly quenching (Bernasconi pers. comm. 2014) agrees with the extrapolation of our low temperature calibration. Moreover, the UEA calibration is, within measurement error, in agreement with the calibrations of Petrizzo *et al.*, 2014 and the subset of samples analysed by Kelson *et al.* (2017) in which samples were reacted at the same temperature as used in this study, i.e. 25°C. The calibration of Kelson *et al.*, (2017) extends to 90°C and covers the range of temperatures reported in this study. Maximum differences of 10°C are observed for estimated temperatures using the UEA and Kelson *et al.* (2017) calibrations. Similarly, a comparison between our calibration, and that of Kluge *et al.* (2015) that covers the temperature range 23-250°C and referenced to a 25°C reaction temperature show the calibrations to be in agreement within experimental error. The UEA and the Petrizzo *et al.* (2014), Kluge *et al.* (2015) and Kelson *et al.* (2017) calibrations lie very close to the theoretical estimates of the temperature dependence of heavy isotope clumping in  $\text{CO}_2$  analyte gas produced by reaction of calcite with phosphoric acid at 25°C (Schauble *et al.* 2006; Guo *et al.* 2009). We consider that these observations indicate that the UEA calibration is robust over the range of temperatures encountered in this study.

## Results

The data for bulk and clumped isotope analysis of all samples and standards are reported in Table 1 and plotted in Figures 4 and 5. Data for the  $\Delta_{48}$  value are included in Table 1. We use  $\Delta_{48}$  to assess for the possibility of sample contamination and thus non-representative  $\Delta_{47}$  values. For all the samples  $\Delta_{48}$  values are close to zero and usually slightly negative with respect to the mass spectrometer working reference gas. This is good evidence that the sample analyte gases are not contaminated (e.g.

Huntington *et al.* 2009).

The variation in isotope values and temperature  $T(\Delta_{47})$  along the growth direction of the vein are plotted in Figure 4 (a) and (b) for DLR7-a and DLR7-b respectively. The two sections were cut at different locations across the vein and have been measured with respect to different zero datums. Thus, we don't a-priori expect a direct correlation between them. There are, however, similarities. DLR7-a has a distinctive, repeating asymmetric saw-tooth pattern along the growth direction that is most marked for  $\delta^{18}\text{O}$  and  $T(\Delta_{47})$ . Four regions of section DLR7-a, separated by the grey bands in Figure 4(a), are identified. The bands mark negative step changes in  $T(\Delta_{47})$  between adjacent areas of the transect. Each area is characterized by a rising temperature from a minimum of  $40^\circ$  to a maximum of  $90^\circ\text{C}$ . This pattern is mirrored by antithetic changes in  $\delta^{18}\text{O}$ , falling from a maximum value of  $-8\text{‰}$  to a minimum of  $-10\text{‰}_{\text{VPDB}}$ . Unlike for  $\delta^{18}\text{O}$  and  $T(\Delta_{47})$  there is no consistent pattern of variation for  $\delta^{13}\text{C}$  with values ranging between  $+1.5$  and  $+3.8\text{‰}_{\text{VPDB}}$ .

The asymmetric, sawtooth pattern observed in section DLR7-a is not readily apparent in section DLR7-b. It is still possible, however, to identify regions where there is a marked pattern of variation, notably for  $\delta^{18}\text{O}$ , Figure 4 (b). For example, between 10 and 20, 55 and 60 and 65 and 75mm there is a fall in the  $\delta^{18}\text{O}$  value that is mirrored by a rise in  $T(\Delta_{47})$ . Between 25 and 50mm there is an apparent breakdown in the inverse relationship between  $T(\Delta_{47})$  and  $\delta^{18}\text{O}$ . In this region temperatures for the most part are greater than  $70^\circ\text{C}$  whilst  $\delta^{18}\text{O}$  remains constant and close to  $-9.8\text{‰}_{\text{VPDB}}$ . We shall return to this apparent lack of variation of  $\delta^{18}\text{O}$  towards the higher temperature range reported here in the discussion. As with section DLR7-a the carbon isotope data does not show a marked covariation with either temperature or oxygen isotope composition and the range of measured values is identical between  $+1.5$  and  $+3.8\text{‰}_{\text{VPDB}}$ .

On a plot of  $\delta^{13}\text{C}$  versus  $\delta^{18}\text{O}$  the restricted range of isotopic composition of the vein is highlighted with  $\delta^{13}\text{C}$  and  $\delta^{18}\text{O}$  values between  $+1.5$  to  $+3.7\text{‰}_{\text{VPDB}}$  and  $-7$  to  $-10\text{‰}_{\text{VPDB}}$  respectively, Figure 5 (a). There is a degree of structure in the data. For the most part  $\delta^{18}\text{O}$  and  $\delta^{13}\text{C}$  are decoupled with a horizontal band of compositions covering a range of  $\delta^{18}\text{O}$  values between  $-8$  and  $-10\text{‰}_{\text{VPDB}}$  and little or no variation in  $\delta^{13}\text{C}$  at a value close to  $+3.5\text{‰}_{\text{VPDB}}$ . A subset of the data with a positive 1:1 correlation between  $\delta^{13}\text{C}$  and  $\delta^{18}\text{O}$  and an outlier of three points with relatively high  $\delta^{18}\text{O}$  values ( $-7$  to  $-8\text{‰}_{\text{VPDB}}$ ) and low  $\delta^{13}\text{C}$  values ( $1.5$  to  $2\text{‰}_{\text{VPDB}}$ ) is evident.

Whilst the lowest temperature vein calcite does have the lowest  $\delta^{13}\text{C}$  value ( $32^\circ\text{C}$  and  $1.6\text{‰}_{\text{VPDB}}$ ) there is no overall correlation between temperature and carbon isotopic composition, Figure 5 (b). In contrast there is a clear inverse covariation between  $T(\Delta_{47})$  and  $\delta^{18}\text{O}$ . A change in precipitation temperature from  $30^\circ$ - $100^\circ\text{C}$  is accompanied by a near  $3\text{‰}$  decrease in the  $\delta^{18}\text{O}$  value of the vein calcite from  $-7$  to  $-10\text{‰}_{\text{VPDB}}$ , Figure 5 (c).

Using the measured  $T(\Delta_{47})$  and  $\delta^{18}\text{O}$  values we have calculated the composition of the fluid that is in theoretical isotopic equilibrium with the vein calcite. For this we used the Kim and O'Neill (1996) calibration of the calcite-water fractionation factor. The data plotted in Figure 5 (d) show a marked linear covariation that resembles a two end-member mixing line. Data for the two sections DLR7-a and DLR7-b plot as similar trends within measurement error. At the high temperature end the calcite is in equilibrium with water at  $100^\circ$ - $110^\circ\text{C}$  and with an enriched  $\delta^{18}\text{O}$  value close to  $+6\text{‰}_{\text{VSMOW}}$ . The low temperature end ( $30^\circ$ - $40^\circ\text{C}$ ) is characterized by more negative values of  $\delta^{18}\text{O}$  between  $-2$  and  $-4\text{‰}_{\text{VSMOW}}$ .  $T(\Delta_{47})$  and the fluid  $\delta^{18}\text{O}$  plotted in Figure 5 (d) are not independent and thus the errors are not orthogonal. We have plotted the 90% error envelope typical of the high and low temperature data and corresponding to a  $\pm 0.014\text{‰}$  ( $1\sigma$ ) and  $\pm 0.1\text{‰}$  precision for  $\Delta_{47}$  and  $\delta^{18}\text{O}$  respectively. This was determined using a monte-carlo simulation of 1000 independent  $\Delta_{47}$  and  $\delta^{18}\text{O}$  pairs. The errors are

dominated by the precision at which  $\Delta_{47}$  can be measured with the first eigen vector of the error ellipse oriented parallel to the isopleths of constant calcite  $\delta^{18}\text{O}$  value. This lends a strong sense of coherence to the observed trend. Not-with-standing this observation the trend is real with a gradient greater than the local slope of the calcite  $\delta^{18}\text{O}$  isopleths. This is emphasized in the inverse covariation of  $T(\Delta_{47})$  and calcite  $\delta^{18}\text{O}$  values plotted in figure 5 (c).

## Discussion

The veins at Dirlow Rake are equivalent to stage 4 of the diagenetic sequence that has been identified in the Visean carbonates of the Peak District (Walkden & Williams 1991; Hollis and Walkden 2002). These authors suggest they represent the later stages of burial diagenesis, precipitating from fluids that are sourced from the sedimentary basins surrounding the Derbyshire Platform. The range of  $\delta^{13}\text{C}$  and  $\delta^{18}\text{O}$  values for zone 4 calcites reported by Hollis and Walkden (2002) for the northern margin of the platform is coincident with those we report here. The positive  $\delta^{13}\text{C}$  values ( $\approx +3$  to  $+4\text{‰}_{\text{VPDB}}$ ) and moderately depleted  $\delta^{18}\text{O}$  values ( $\approx -7$  to  $-10\text{‰}_{\text{VPDB}}$ ) are consistent with precipitation from warm formation fluids that have evolved with low water to rock ratios under closed system conditions. We develop these ideas in the discussion using data for the clumped isotope temperature to constrain the likely source of the mineralizing fluids and outline a simple two component mixing process between formation waters from the Edale Basin and groundwaters local to the site of mineralization. We identify a temperature anomaly associated with the upwelling hot waters along the Dirlow Rake fault and use a simple thermal model to estimate the necessary rates of fluid migration required to sustain the temperature anomaly. Finally, we attempt a synthesis of the data in terms of a simple basin evolution model, the development of overpressure as a possible result of gas generation and the initiation of seismic activity and subsequent fluid flow along high permeability rupture zones i.e. a seismic valve.

## Temperature

The data for the temperature at which calcite precipitated at Dirlow Rake are the first measurements made for the southern Pennines using the clumped isotope technique. They show that temperatures varied during vein growth between lower and upper limits of  $30^\circ\text{C}$  and  $100^\circ\text{C}$ . The temperature varies in a systematic and episodic manner. It is relevant to ask if these temperatures are robust and representative of the likely hydrothermal fluid temperatures. The most direct comparison we can make is with fluid inclusion homogenization temperatures.

Hollis and Walkden (2002) report a mean temperature of  $154^\circ\text{C}$  with a large range of between  $100^\circ$  and  $200^\circ\text{C}$  for inclusions in zone 4 calcites sampled from the northern margin of the Derbyshire platform. Higher maximum temperatures and a greater temperature range have been reported by Kendrick *et al.* (2002) for fluorites from Hucklow Edge, a mineralized vein within 10km of Dirlow Rake ( $T_{\text{max}} = 240^\circ\text{C}$ , range =  $90^\circ$ - $240^\circ\text{C}$ ). These authors exclude reported temperatures as high as  $300^\circ\text{C}$  suggesting the data are compromised by stretching and fluid loss from the inclusions. All these values are significantly higher than the temperature range we report here and higher than any temperatures we have recorded using clumped isotopes elsewhere in the Peak District (unpublished data). The high maxima and large range of temperatures reported by Hollis and Walkden (2002) and Kendrick *et al.* (2002) are hard to reconcile with the clumped isotope data. They are also hard to understand in relation to current models for evolution of the platform and surrounding basins. Maximum temperatures on the platform are thought not to exceed  $70^\circ$ - $100^\circ\text{C}$  with maximum

temperature of fluids sourced from the basin sediments of 200 °C (Colman *et al.* 1989; Walkden & Williams 1991; Andrews 2013). A possible explanation for the discrepancy between clumped isotope and calcite fluid inclusion homogenization temperatures is that the inclusions may be gas rich. Such gas rich inclusions result from phase separation as a result of effervescence at the time of mineralization with apparently high temperatures previously reported from carbonate phases from MVT districts (Jones & Kesler 1992). The gas phase forms by vapour separation due to over-pressured fluids migrating into areas of hydrostatic pressure. Homogenisation temperatures measured for such inclusions are significantly greater than the true temperatures prevailing at the time of mineral growth (Jones & Kesler, 1992).

In contrast the clumped isotope temperature data are in close to good agreement with other fluid inclusion studies for samples from the Peak District orefield. Atkinson (1983) reported homogenization temperatures in the range 62°-157 °C for primary and pseudo-secondary inclusions in fluorite from the southern Pennine orefield (type 1 = 119.5° - 157 °C; type 2 = 62° - 82 °C; type 3 = 64.9° - 98.9 °C; type 4 = 63.4° - 106 °C and type 5 = 66.3° - 68.3 °C). Masheded and Rankin (1988) measured homogenization temperatures of between 58° and 97 °C for fluid inclusions in calcite and fluorite from the Ecton Hill copper deposit on the south-western edge of the Derbyshire platform.

A similar broad agreement between temperatures estimated using fluid inclusion homogenization and the clumped isotope thermometer has been reported by Came *et al.* (2017) for dolomites from the Lower Ordovician of western Newfoundland. Though, philosophically the Came *et al.* study used fluid inclusion homogenization temperatures as an independent variable in an experiment to calibrate the clumped isotope thermometer for dolomite at elevated temperatures. Comparing these temperatures with clumped isotope temperatures estimated using a  $\Delta_{47}$ -T calibration that is essentially identical to ours the spread of the data shows some inclusion temperatures to be higher than those estimated using  $\Delta_{47}$  whilst others are significantly lower (ca. 50 °C) (cf. Figure 5 (Came *et al.* (2017))).

In conclusion the clumped isotope temperatures are in agreement with the reported lower estimates of inclusion homogenization temperatures but significantly lower than the highest reported temperatures for the Derbyshire ore field.

## Fluid isotope compositions, sources and mixing processes

We have suggested that the linear covariation of temperature and fluid isotope composition revealed in Figure 5(d) represents a two-component mixing line with hot and cool end members. The hot end member has a temperature >100 °C and a  $\delta^{18}\text{O}$  value of approximately +5‰ to +6‰<sub>VSMOW</sub> whilst the cool end member has a temperature of 30° to 45 °C and a  $\delta^{18}\text{O}$  value of -2 to -4‰<sub>VSMOW</sub>.

The isotopic composition of the low temperature end member, depleted in  $^{18}\text{O}$  with respect to ocean water, is typical of meteoric groundwaters. The range of minimum temperatures (30°-50 °C) is likely to be characteristic of the depth of burial at the time of mineralization and thus the near surface hydrogeology of the platform carbonates was dominated by meteoric recharge. With an elevated geothermal gradient of between 40° to 50 °C km<sup>-1</sup> this suggests that mineralization could have occurred at depths of 0.8 to 1km. This is shallower than depths of 1 to 2km suggested by previous studies (e.g. Colman *et al.* 1989).

The high temperature end member has a temperature greater than 100 °C and a  $\delta^{18}\text{O}$  value of +5‰<sub>VSMOW</sub>. Such temperatures and fluid isotope compositions are typical of many sedimentary basin and oil field brines (Sheppard 1986). The fluid is most probably sourced from depth within the Viséan-Namurian shales of the Bowland-Hodder unit in the Edale Gulf. Likely minimum source

depths are between 2 to 3 km. An interesting comparison can be made between the formation water isotope composition of  $+5\text{‰}_{\text{VSMOW}}$  and that expected for a fluid in isotopic equilibrium at temperature with shales containing clay minerals. In Figure 6 we have replotted the data of Figure 5(d) and included the fields of end-member compositions. Also plotted is the trajectory of evolution of pore waters in a shale assuming: (i) the pore waters are connate and have an initial marine isotope composition of  $0\text{‰}_{\text{VSMOW}}$ ; (ii) the system evolves under closed system conditions with a porosity of 20%; (iii) isotopic equilibrium is attained between the clay minerals and pore water and; (iv) the initial  $\delta^{18}\text{O}$  value of the kaolin in the shale is  $+20\text{‰}_{\text{VSMOW}}$ . The oxygen isotope fractionation factors for the kaolin-water system is taken from Sheppard and Gilg (1996).

At a temperature of  $100^{\circ}$  to  $115^{\circ}\text{C}$  a pore fluid in equilibrium with the shale has a  $\delta^{18}\text{O}$  value of  $\approx 5\text{‰}_{\text{VSMOW}}$  in good agreement with the derived fluid isotope composition determined using  $T(\Delta_{47})$  and the  $\delta^{18}\text{O}$  value of the vein calcite. The assumptions we have made in this calculation are reasonable. Bulk rock isotope values for shales are close to  $+20\text{‰}_{\text{VSMOW}}$ . Moreover, using the excess He content of fluids trapped in fluid inclusions Kendrick *et al.* (2002) have estimated typical pore water residence times within the shales for the Edale Gulf fluids of as much as 50Ma allowing plenty of time for the pore water to come to thermal and isotopic equilibrium with detrital and authigenic clay minerals.

In contrast fluids that are theoretically in isotope equilibrium with the host Dinantian limestones at high temperature are more enriched in  $^{18}\text{O}$  by between 4 and 8‰ depending on the  $\delta^{18}\text{O}$  value assumed for typical Dinantian marine limestones. Altered whole rock values are close to  $-6\text{‰}_{\text{VPDB}}$  whilst the least altered bioclastic components of the limestones have values as high as  $-2\text{‰}_{\text{VPDB}}$  (Walkden & Williams 1991).

We are reassured that the derived fluid  $\delta^{18}\text{O}$  values are consistent with our understanding of the isotopic compositions of naturally occurring fluids and suggests that the clumped isotope temperatures are robust. For example, were the calcite temperatures to have been as high as the maximum reported fluid inclusion homogenization temperatures of  $240^{\circ}\text{C}$  then the derived fluid  $\delta^{18}\text{O}$  values would need to have been in excess of  $+18$  to  $+20\text{‰}_{\text{VSMOW}}$ . Such large values are typically in excess of any reported data for modern geothermal and formation waters (Sheppard 1986).

Finally, note that at temperatures greater than approximately  $70^{\circ}\text{C}$  the gradient of the mixing line defined by the data is close to that of the isopleths of constant carbonate  $\delta^{18}\text{O}$  values that are defined by the equilibrium fractionation of  $^{18}\text{O}$  between calcite and water (Kim & O'Neill 1997). This accounts for the observation that towards the higher temperature range there is a break down in the inverse relationship seen between temperature and  $\delta^{18}\text{O}$  noted in the vein transect DLR-7b and the  $T(\Delta_{47})$  versus  $\delta^{18}\text{O}$  plot, Figure 5(c).

In Figure 7 we have taken the data plotted in Figure 5(c) and superposed two trends. The first is for the expected composition of calcite precipitated from a fluid produced by conservative mixing of a high temperature formation water and a meteoric groundwater. The two fluid compositions were determined from the line of best fit to the data in Figure 5(c) and assuming cold and hot end member temperatures of  $30^{\circ}$  and  $100^{\circ}\text{C}$ . The second trend line describes the expected calcite oxygen isotope compositions that result from precipitation from a fluid cooling from the high temperature end member composition. The data are consistent with the mixing model and clearly at variance with precipitation from a cooling high temperature fluid.

The mixing model provides a process to account for the repeated cycles of isotope change seen along the growth axis of the vein, notably for transect DLR7-a, Figure 4. Here we see a repeated pattern of warming accompanied by a decrease in the oxygen isotope composition of the precipitated calcite.

This trend is abruptly terminated with a return to cooler conditions accompanying calcite growth. A scenario to account for this pattern is the upward flow of formation water along a high permeability fault plane. During ascent the fluid will mix with the local groundwater. The variable mixing ratio is determined by the relative fluxes of the two components into the fault zone. The flow of formation waters could be driven by overpressure in the deep fault-bounded sedimentary basins. Increasing rates of formation water release, leading to increased temperatures of precipitation, could be related to a pore fluid pressure sensitivity of the shale permeability (Rutter *et al.* 2013). Moreover, transmission of pore fluid pressures associated with catastrophic rupture of capillary seals in the shales (Cathles 2007) may also initiate fault activity through reduction of the normal stresses across slip planes. At a critical fluid pressure the fault ruptures, pore fluid pressure rapidly dissipates and the efflux of formation water decreases resulting in the stepped temperature and isotopic profiles observed in the vein. Such a process is closely aligned to the seismic valve model for faulting and fluid release described by Sibson (1981).

### Thermal constraints on fluid flux

A requirement of the mixing model is that fluid ascent is fast enough such that heat is largely retained in the fluid and temperature can be used as a conservative tracer for the two components. To a first approximation we can use the estimated temperatures of the fluid end members to constrain the flux of fluid needed to develop a thermal anomaly similar to that observed at Dirlow Rake. The question is how much fluid and how fast does it have to flow along the fault to (i) heat the rock in the fault zone and (ii) prevent significant heat loss via conduction through the walls of the fault? The problem is illustrated in Figure 8.

Hydrothermal fluid at an initial temperature  $\Theta_1$  enters the fault at depth  $x_1$  where the temperature due to the local geothermal gradient is  $\Theta_1$ . The fluid flows up along the fault to a depth of  $x_2$  where the local temperature is  $\Theta_2$ . We assume that the heat lost from the fluid is partitioned into two components:

(i) heats the immediate fault zone between depths  $x_1$  and  $x_2$  to the temperature  $\Theta_1$  ( $\Delta H_a$ ),

$$DH_a = (x_1 - x_2) \cdot h \cdot \left( \frac{Q_1 - Q_2}{2} \right) \cdot C_p^r \cdot \rho^r \quad (12)$$

where  $h$  is the effective width of the fault,  $C_p^r$  and  $\rho^r$  are the specific heat capacity and density of the rock;

(ii) is lost through thermal diffusion perpendicular to the fault walls ( $\Delta H_b$ ). For a parallel plate slab (Crank 1975, eqn. 3.15),

$$DH_b = (x_1 - x_2) \cdot (Q_1 - Q_2) \cdot \left( \frac{kt}{\rho} \right) \cdot C_p^r \cdot \rho^r \quad (13)$$

where  $k$  is the thermal diffusivity of rock and  $t$  is the time over which heat is conducted away from the fault. Thus the energy balance per metre length of fault can be expressed as,

$$V \cdot (Q_1 - Q_2) \cdot C_p^w \cdot \rho_w = DH_a + DH_b \quad (14)$$

where  $V$  is the volume of fluid expelled along the fault,  $C_p^w$  and  $\rho_w$  are the specific heat capacity and density of water respectively. Noting that  $C_p^w \cdot \rho_w \approx 2 \cdot C_p^r \cdot \rho_r$  and selecting values of  $120^\circ$ ,  $100^\circ$  and  $40^\circ\text{C}$  respectively for  $\Theta_i$ ,  $\Theta_1$  and  $\Theta_2$ , 3000m for  $x_1$ , 1000m for  $x_2$  and a thermal conductivity of  $1 \times 10^{-6} \text{ m}^2 \text{ s}^{-1}$  we find that the maximum duration (s) for an individual fluid pulse is:

$$t = \frac{\rho \cdot \left( 3.3 \times 10^{-4} \cdot V - \frac{h}{2} \right)^2}{1 \times 10^{-6}} \quad (15)$$

Table 2 lists values of  $t$  for different values of  $V$ , the volume of fluid released along the fault zone and for  $h$ , the effective width of the fault zone. The values of  $V$  were chosen corresponding to the volumes of fluid expelled from an overpressured 40km wide x 2km thick sediment sequence at depth with incremental changes in porosity of 0.1, 1 and 10% on dewatering. These dimensions approximate to the width and thickness of shale in the Carboniferous Edale basin immediately to the north-east of the Derbyshire platform. The porosity changes range from the smallest incremental changes calculated for individual dewatering pulses of overpressured sediments to the integrated maximum volume of fluid that might be expelled (Cathles 1983). The corresponding values of  $t$  for a fault width of 1m are 68, 6912 and 694000 years respectively. These correspond to mean effusive fluxes,  $J$ , of 136, 13.2 and 1.3 litres  $\text{hr}^{-1}$  for every metre length of the fault. There are only minor changes in the estimated values of  $t$  and  $J$  if we carry out the same calculation for a 10m fault width. The flow rates listed in Table 2 are geologically realistic. The highest fluxes are associated with the lowest volume fluid pulses and are on the order of the rates of effusion from springs that have been monitored for periods of several years following moderate earthquakes e.g Nur (1974) and Tsuneishi *et al.* (1970). Moreover, assuming overpressures similar to the lithostatic minus the hydrostatic pressure gradient such flows would require fault zone permeabilities of  $10^{-12}$  to  $10^{-15} \text{ m}^2$ . Such permeabilities have been measured in fault zones in carbonate terrains (e.g. Micarelli *et al.* 2006)

One can legitimately question the model details and parameter estimates but the point of this somewhat heuristic approach is not to be accurate. Rather, it is to give an approximate indication of the flow rates that are needed to sustain the maximum observed thermal anomaly within the Dirlow Rake fault and to assess whether these are reasonable. That the model may only be accurate to within a factor of 5 to 10 does not invalidate the central result that if fluid release occurs in a pulsed and episodic manner then each event must be of short duration to sustain the necessary thermal anomaly. The duration of these events and maximum flow rates associated with them are commensurate with fluid fluxes associated with contemporary observations of fluid behaviour following earthquake rupture.

Basin-wide gravity driven flow through the Bowland-Hodder shale unit as a result of surface topography (e.g. Ford & Worley 2016; Quirk 1993) with discharge along fault traces cannot provide the necessary fluid fluxes to develop and sustain the temperature anomalies that we report here. Flow is limited by both the maximum hydraulic gradients that could be developed and relatively low intrinsic permeabilities of the Bowland-Hodder unit in the Edale Gulf.

In a wider context the conclusions we reach about the pulsed and rapid nature of fluid flow at Dirtlow Rake and possibly in the wider Peak District MVT system are convergent with ideas expressed by several researchers in which the time scale for fluid flow and overall volumes of fluids involved in the mineralization are very much reduced (e.g. Cathles & Smith 1986; Bodnar 2009; Wilkinson *et al.* 2009). They pose serious questions about our understanding concerning the transport and precipitation of carbonate minerals in fracture systems. For example modelling and experimental data on vein formation suggest that an extremely large volume of fluid is required to produce calcite veins in nature with fluid:calcite volume ratios of  $10^5$  to  $10^6$ . These same models also predict that the flow needs to be sustained for thousands to millions of years (Lee *et al.* 1996; Lee & Morse 1999).

## Synthesis

In Figure 9 we present a basin development model for the Derbyshire Platform and the Edale Gulf. The model is based on that of Colman *et al.* (1989) and Walkden and Williams (1991), with the addition of time lines for the evolution of mineralizing fluids and mineralization based on published geochemical data and the results of this study. Basin evolution through the Mesozoic and Cenozoic allows for the development of as much as 1.4km of Mesozoic cover on top of the platform (Hillis *et al.* 2008). The Visean-Namurian boundary in both the Edale Gulf and on the Derbyshire platform is shown. The isotherms are as described in Colman *et al.* (1969) and Walkden and Williams (1991) with geothermal gradients approaching  $40^{\circ}$ - $50^{\circ}\text{C km}^{-1}$  at the time of maximum basin depth towards the end of the Carboniferous. The high geothermal gradient is consistent with heat flows in excess of  $70\mu\text{W m}^{-2}$  that have been modelled for the end of the Carboniferous in the nearby Widmerpool Gulf and Gainsborough Trough basins (Anderson 2013). The timing of mineralization is based on K-Ar dates of 270Ma for hydrothermally altered doleritic lavas and pumice tuffs adjacent to mineralized areas in Derbyshire (Ineson & Mitchell 1972). If the mineralizing fluids are sourced from the Bowland-Hodder shales in the Edale Gulf basin then these ages are consistent with the excess  $^4\text{He}$  found in fluid inclusion waters which suggests a residence time in excess of 50Ma (Kendrick *et al.* 2002).

We suggest that sediment compaction and high gas pressures led to significant over-pressures in the Bowland-Hodder shale. In the interval 325 to 280-270Ma the Edale Gulf underwent rapid subsidence with the top of the Visean reaching a maximum depth of 3km and temperatures close to  $150^{\circ}\text{C}$ . Sediments in the basin passed through the oil and gas generation windows with production of large volumes of shale gas. In addition, diagenesis of clay rich sediments can also lead to the production of high over pressures of  $\text{CO}_2$  (Hutcheon & Desrochers 2003). In the presence of two-phase gas-liquid pore fluids the system can become highly compartmentalized with the development of tight capillary seals and overpressured sediments (Cathles & Adams 2005; Cathles 2007).

At high pore fluid pressures effective stress dependent shale permeability (Rutter *et al.* 2013) may allow increasing rates of leakage of the pore fluid. If the pressures are not dissipated through such leakage and continue to rise failure of capillary seals could result in a gas pulsar (Cathles 2007) with rapid expulsion of trapped fluids and gas and rapid displacement of large volumes of fluid in the more

permeable units of the sediment pile. This may result in transmission of high pore fluid pressures into the fault zone promoting failure as a result of the reduction in effective stresses on the fault surface. The rapid and episodic expulsion of gas and fluids from the shale units with flow focused along high permeability fault zones would allow for the dissipation of pressure in over-pressured cells within the shale 'switching-off' the flow. Importantly, repeated catastrophic failure of capillary seals does not require the constant generation of gas and could be triggered by uplift and reduction of the overburden pressure during the Variscan inversion, Figure 9. During uplift pockets in the shale units with significant gas overpressure will intercept the lithostatic pressure curve and fail.

This model has similar characteristics to that proposed by Frazer *et al.* (2014) for mineralization in the southern Pennines with catastrophic de-watering of overpressured shales as a result of faulting. The key difference is that we present evidence for episodic pulses of rapidly ascending fluids whereas the Frazer *et al.* (2014) model envisages compaction driven dewatering of over-pressured basin sediments during a ca. 10Ma period from 310 to 300Ma at the time of maximum basin depth.

Finally, we note that there is abundant evidence for a close association between hydrocarbons and mineralization in the Peak District e.g. Moser and Rankin (1992) and Ewbank *et al.* (1995) as well as globally. More recently Cathles and Adams (2005) and Cathles (2007) have suggested that basin centred gas deposits and gas pulsars may provide an explanation *sensu lato* for many of the enigmatic characteristics of MVT deposits and notably their episodic and pulsed nature and the evidence for a distinct thermal anomaly in which mineralization temperatures are elevated compared to the host rock temperatures.

## Conclusion

We present new clumped isotope thermometry data for vein calcite associated with Dirlow Rake, a mineralized strike slip fault that is closely associated with the Castleton fault system that bounds the lower Carboniferous Derbyshire platform and adjacent Edale Gulf. We find that:

1. the calcite precipitated at temperatures between 40° and 100°C.
2. the parent fluids range in isotopic composition from -4 to +5‰<sub>VSMOW</sub> and represent mixtures of a cool meteoric water and a more evolved formation water.
3. the temperature at which the calcite precipitated is a conservative tracer for the fluid mixing. This implies that heat is rapidly advected as the hydrothermal fluid flow is focussed along the fault plane.
4. The calcites exhibit zoned development characterized by cyclic and pulsed evolution of precipitation temperatures and fluid compositions resulting from a range of mixing ratios of the two fluid end members.
5. The high temperature formation water may be connate and has evolved under low fluid:rock ratios and is in equilibrium with the siliciclastic basin fill.

Simple thermal considerations indicate that fluid flow was episodic and highly focussed along the fault plane. We conclude that rising pore fluid pressures as a result of rapid sedimentation, hydrocarbon generation and silicate diagenesis coupled with changing tectonic and overburden stresses as the basin inverted during the Variscan orogeny led to hydraulic fracturing of the basin

shales, fault movement and release of the pore fluid pressure as the sediment pile dewater. As with the example of the upper Mississippi Valley sedimentary basins the dewatering is episodic with extended periods during which the pore fluid pressure increases. These periods are punctuated by short duration episodes of fluid release. This resembles very closely a seismic valve type process in which rising pore fluid pressure reduces the effective stress on fault surfaces, ultimately leading to failure and the formation of a high permeability path along which the pore fluid is released and the pressure dissipated.

**Acknowledgements:** PFD is grateful to the University of East Anglia who supported financially and academically the design, construction and development of the MIRA mass spectrometer and sample processing system. Dave Harbour provided invaluable engineering advice and carried out the machining of components for the mass spectrometer. The temperature calibration study was part of RK's PhD thesis and the analyses of vein carbonates was completed as part of DJM's MSci course work research dissertation in stable isotope geochemistry. Finally, we acknowledge the very thoughtful and constructive comments of Kate Huntington and an anonymous reviewer which has helped clarify some of our ideas and improved the paper.

## References

- Andrews, I. J. 2013. *The Carboniferous Bowland Shale gas study: geology and resource estimation*, British Geological Survey for Department of Energy and Climate Change, London, UK, 56pp.
- Atkinson, P. 1983. *A fluid inclusion and geochemical investigation of the fluorite deposits of the southern Pennine orefield*. PhD thesis, University of Leicester.
- Baertschi, P. 1976. Absolute  $^{18}\text{O}$  content of standard mean ocean water, *Earth and Planetary Science Letters*, **31**, 341–344, [http://doi.org/10.1016/0012-821X\(76\)90115-1](http://doi.org/10.1016/0012-821X(76)90115-1)
- Barnett, J. 2002 Excavation and conservation at How Grove, Dirlow Rake, Castletown, Derbyshire, *The Bulletin of the Peak District Mines Historical Society*, **15**, 1-40.
- Bergman, S. C., Huntington, K. W., & Crider, J. G. 2013. Tracing paleofluid sources using clumped isotope thermometry of diagenetic cements along the Moab Fault, Utah, *American Journal of Science*, **313**, 490–515, <http://doi.org/10.2475/05.2013.03>
- Bodnar, R. J. 2009. Heavy Metals or Punk Rocks?, *Science*, **323**, 724–725.
- Brand, W.A., Assonov, S.S., & Coplen, T.B., 2010. Correction for the  $^{17}\text{O}$  interference in  $\delta(^{13}\text{C})$  measurements when analyzing  $\text{CO}_2$  with stable isotope mass spectrometry (IUPAC technical report), *Pure and Applied Chemistry*, **82**, 1719-1733
- Came, R.E., Azmy, K., Tripathi, A., & Olanipekun, B-J., 2017. Comparison of clumped isotope signatures of dolomite cements to fluid inclusion thermometry in the temperature range of 73-176°C, *Geochimica et Cosmochimica Acta*, **199**, 31-47, <http://dx.doi.org/10.1016/j.gca.2016.10.028>
- Cathles, L. M. & Smith, A. T. 1983. Thermal Constraints on the Formation of Mississippi Valley-Type Lead-Zinc Deposits and Their Implications for Episodic Basin Dewatering and Deposit Genesis, *Economic Geology*, **78**, 983–1002.

- Cathles, L.M. and Adams, J.J. 2005. Fluid flow and petroleum and mineral resources in the upper (< 20 km) continental crust. *Economic Geology*, 100th Anniversary Volume, pp.77-110.
- Cathles, L. M. 2007. Changes in sub-water table fluid flow at the end of the Proterozoic and its implications for gas pulsars and MVT lead-zinc deposits, *Geofluids*, **7**, 209–226, <http://doi.org/10.1111/j.1468-8123.2007.00176.x>
- Charef, A. & Sheppard, S. 1988. The Malines Cambrian carbonate-shale-hosted Pb-Zn deposit, France: Thermometric and isotopic (H, O) evidence for pulsating hydrothermal mineralization, *Mineralium Deposita*, **23**, 86–95.
- Colman, T. B., Cornwell, J. D., Jones, D. G., Lafolley, N. D., Walker, A. S. D., Smith, K., et al. (1989). Metallogenic models and exploration criteria for buried carbonate-hosted ore deposits - a multidisciplinary study in eastern England. (J. A. Plant & D. G. Jones, Eds.) (pp. 1–184). The Institution of Mining and Metallurgy.
- Crank, J. 1975. *The Mathematics of Diffusion*, Oxford University Press, 414pp.
- Cruset, D., Cantarero, I., Travé, A., Vergés, J., & John, C. M. (2016). Crestal graben fluid evolution during growth of the Puig-reig anticline (South Pyrenean fold and thrust belt). *Journal of Geodynamics*, 101, 30–50. <http://doi.org/10.1016/j.jog.2016.05.004>
- Daëron, M., Blamart, D., Peral, M., & Affek, H. P. (2016). Absolute isotopic abundance ratios and the accuracy of  $\Delta 47$  measurements. *Chemical Geology*, 442, 83–96. <http://doi.org/10.1016/j.chemgeo.2016.08.014>
- Dennis, K. J. & Schrag, D. P. 2010. Clumped isotope thermometry of carbonatites as an indicator of diagenetic alteration. *Geochimica et Cosmochimica Acta*, **74**, 4110–4122, <http://doi.org/10.1016/j.gca.2010.04.005>
- Dennis, K. J., Affek, H. P. et al. 2011. Defining an absolute reference frame for “clumped” isotope studies of CO<sub>2</sub>, *Geochimica et Cosmochimica Acta*, **75**, 7117–7131, <http://doi.org/10.1016/j.gca.2011.09.025>
- Eiler, J. M. 2007. “Clumped-isotope” geochemistry—The study of naturally-occurring, multiply-substituted isotopologues, *Earth and Planetary Science Letters*, **262**, 309–327.
- Ewbank, G., Manning, D. A. C., & Abbott, G. D. 1995. The relationship between bitumens and mineralization in the South Pennine Orefield, central England. *Journal of the Geological Society*, **152**, 751–765, <http://doi.org/10.1144/gsjgs.152.5.0751>.
- Ford, T. D. & Worley, N. E. 2016. Mineralization of the South Pennine Orefield, UK—A Review. *Proceedings of the Yorkshire Geological Society*, **61**, 55–86. <http://doi.org/10.1144/pygs2015-364>
- Frank, F. C. 1965. On dilatancy in relation to seismic sources. *Reviews of Geophysics*, **3**, 485–503.
- Frazer, M., Whitaker, F. & Hollis, C. 2014. Fluid expulsion from overpressured basins: Implications for Pb–Zn mineralization and dolomitisation of the East Midlands platform, northern England. *Marine and Petroleum Geology*, **55**, 68–86, <http://doi.org/10.1016/j.marpetgeo.2014.01.004>
- Garven, G., & Freeze, R. A. 1984. Theoretical-Analysis of the Role of Groundwater-Flow in the Genesis of Stratabound Ore-Deposits .1. Mathematical and Numerical-Model. *American Journal of Science*, **284**, 1085–1124, <http://doi.org/10.2475/ajs.284.10.1125>

Garven, G., Appold, M. S. *et al.* 1999. Hydrogeologic modeling of the genesis of carbonate-hosted lead-zinc ores. *Hydrogeology Journal*, **7**, 108–126. <http://doi.org/10.1007/s100400050183>

Ghosh, P., Adkins, J. *et al.* 2006.  $^{13}\text{C}$ – $^{18}\text{O}$  bonds in carbonate minerals: A new kind of paleothermometer, *Geochimica et Cosmochimica Acta*, **70**, 1439–1456, <http://doi.org/10.1016/j.gca.2005.11.014>

Green, P. F. 2005. Post-Carboniferous burial and exhumation histories of Carboniferous rocks of the southern North Sea and adjacent onshore UK. *In*: Collinson, J.D., Evans, D.J., Holliday, D.W. & Jones, N.S. (eds) *Carboniferous Hydrocarbon Geology: the southern North Sea and surrounding onshore areas*, Yorkshire Geological Society Occasional Publications, **7**, 25-34

Guo, W., Mosenfelder, J. L. *et al.* 2009. Isotopic fractionations associated with phosphoric acid digestion of carbonate minerals: Insights from first-principles theoretical modeling and clumped isotope measurements, *Geochimica et Cosmochimica Acta*, **73**, 7203–7225, <http://doi.org/10.1016/j.gca.2009.05.071>

Henkes, G. A., Passey, B. H. *et al.* 2013. Carbonate clumped isotope compositions of modern marine mollusk and brachiopod shells *Geochimica et Cosmochimica Acta*, **106**, 307–325, <http://doi.org/10.1016/j.gca.2012.12.020>

Henley, R. W. & Berger, B. R. 2000. Self-Ordering and Complexity in Epizonal Mineral Deposits, *Annual Reviews of Earth and Planetary Sciences*, **28**, 669–719

Hillis, R. R., Holford, S. P. *et al.* 2008. Cenozoic exhumation of the southern British Isles, *Geology*, **36**, 371–4, <http://doi.org/10.1130/G24699A.1>

Hodson, K. R., Crider, J. G., & Huntington, K. W. (2016). Temperature and composition of carbonate cements record early structural control on cementation in a nascent deformation band fault zone: Moab Fault, Utah, USA. *Tectonophysics*, 690, 240–252. <http://doi.org/10.1016/j.tecto.2016.04.032>

Hollis, C. & Walkden, G. 2002. Reconstructing Fluid Expulsion and Migration North of the Variscan Orogen, Northern England, *Journal of Sedimentary Research*, **72**, 700–710, <http://doi.org/10.1306/012102720700>

Hubbert, M. K. & Rubey, W. W. 1959. Role of fluid pressure in mechanics of overthrust faulting i. mechanics of fluid-filled porous solids and its application to overthrust faulting, *Geological Society of America Bulletin*, **70**, 115–166, <http://doi.org/10.1130/0016-7606>

Huntington, K. W., Eiler, J. M. *et al.* 2009. Methods and limitations of “clumped”  $\text{CO}_2$  isotope ( $\Delta_{47}$ ) analysis by gas-source isotope ratio mass spectrometry, *Journal of Mass Spectrometry*, **44**, 1318–1329, <http://doi.org/10.1002/jms.1614>

Huntington, K. W., & Lechler, A. R. (2015). Carbonate clumped isotope thermometry in continental tectonics. *Tectonophysics*, 647-648, 1–20. <http://doi.org/10.1016/j.tecto.2015.02.019>

Hutcheon, I. & Desrochers, S. 2003. Silicate-carbonate reactions in sedimentary systems: fluid composition control and potential for generation of overpressure, *In*: Worden, H. & Morad, S. (eds) *Clay mineral cements in sandstones*, Special publication of the International Association of Sedimentologists, **34**, 161-176.

Ineson, P. R. & Mitchell, J. G. 1972. Isotopic Age Determinations on Clay-Minerals From Lavas and

Tuffs of Derbyshire Orefield, *Geological Magazine*, **109**, 501–512

Ixer, R.A. & Vaughan, D.J. 1993. Lead-zinc-fluorite-baryte deposits of the Pennines, North Wales and the Mendips. In: Patrick, R.A.D. & Polya, D.A. (eds) *Mineralization in the British Isles* (R.A.D. Patrick and D.A. Polya, eds). Chapman and Hall, London, 355–418

Jones, H. D. & Kesler, S. E. 1992. Fluid inclusion gas chemistry in east Tennessee Mississippi Valley-type districts: Evidence for immiscibility and implications for depositional mechanisms, *Geochimica et Cosmochimica Acta*, **56**, 137–154

Kelson, J. R., Huntington, K. W., Schauer, A. J., Saenger, C., & Lechler, A. R. (2017). Toward a universal carbonate clumped isotope calibration: Diverse synthesis and preparatory methods suggest a single temperature relationship. *Geochimica Et Cosmochimica Acta*, 197, 104–131. <http://doi.org/10.1016/j.gca.2016.10.010>

Kendrick, M. A., Burgess, R. *et al.* 2002. Hydrothermal fluid origins in a fluorite-rich Mississippi Valley-Type district: Combined noble gas (He, Ar, Kr) and halogen (Cl, Br, I) analysis of fluid inclusions from the south Pennine ore field, United Kingdom, *Economic Geology*, **97**, 435–451

Kim, S.-T. & O'Neil, J. R. 1997. Equilibrium and nonequilibrium oxygen isotope effects in synthetic carbonates, *Geochimica et Cosmochimica Acta*, **61**, 3461–3475, [http://doi.org/10.1016/S0016-7037\(97\)00169-5](http://doi.org/10.1016/S0016-7037(97)00169-5)

Kirk, R., 2017, Development of clumped isotope techniques and their application to palaeoclimate studies, unpubl. PhD thesis, University of East Anglia, <http://ueaprints.uea.ac.uk/id/eprint/63690>

Kluge, T., John, C. M., Jourdan, A.-L., Davis, S., & Crawshaw, J. (2015). Laboratory calibration of the calcium carbonate clumped isotope thermometer in the 25–250 °C temperature range. *Geochimica Et Cosmochimica Acta*, 157, 213–227. <http://doi.org/10.1016/j.gca.2015.02.028>

Lee, Y.-J. Morse, J. W., & Wiltschko, D. V. 1996. An experimentally verified model for calcite precipitation in veins, *Chemical Geology*, **130**, 203–215, <http://doi.org/10.1016/0009-2541>

Lee, Y. J. & Morse, J. W. 1999. Calcite precipitation in synthetic veins: implications for the time and fluid volume necessary for vein filling. *Chemical Geology*, **156**, 151–170, [http://doi.org/10.1016/S0009-2541\(98\)00183-1](http://doi.org/10.1016/S0009-2541(98)00183-1)

Luetkemeyer, P. B., Kirschner, D. L., Huntington, K. W., Chester, J. S., Chester, F. M., & Evans, J. P. (2016). Constraints on paleofluid sources using the clumped-isotope thermometry of carbonate veins from the SAFOD (San Andreas Fault Observatory at Depth) borehole. *Tectonophysics*, 690, 174–189. <http://doi.org/10.1016/j.tecto.2016.05.024>

Mashedier, R. & Rankin, A. H. 1988. Fluid inclusion studies on the Ecton Hill copper deposits, north Staffordshire, *Mineralogical Magazine*, **52**, 473–482.

Micarelli, L. Benedicto, A. & Wibberley, C. A. J. 2006. Structural evolution and permeability of normal fault zones in highly porous carbonate rocks, *Journal of Structural Geology*, **28**, 1214–1227, <http://doi.org/10.1016/j.jsg.2006.03.036>

Moser, M. & Rankin, A. 1992. Hydrocarbon-bearing fluid inclusions in fluorite associated with the Windy Knoll bitumen deposit, UK, *Geochimica et Cosmochimica Acta*, **56**, 155–168

Nur, A. 1973. Role of Pore Fluids in Faulting, *Philosophical Transactions of the Royal Society of*

London A: *Mathematical, Physical and Engineering Sciences*, **274**, 297–304,  
<http://doi.org/10.1098/rsta.1973.0056>

Nur, A. 1974. Matsushiro, Japan, Earthquake Swarm: Confirmation of the Dilatancy-Fluid Diffusion Model. *Geology*, **2**, 217–221, <http://doi.org/10.1130/0091-7613>

Passey, B. H., & Henkes, G. A. (2012). Carbonate clumped isotope bond reordering and geospeedometry. *Earth and Planetary Science Letters*, 351-352, 223–236.  
<http://doi.org/10.1016/j.epsl.2012.07.021>

Petrizzo, D. A., Young, E. D. & Runnegar, B. N. 2014. Implications of high-precision measurements of <sup>13</sup>C-<sup>18</sup>O bond ordering in CO<sub>2</sub> for thermometry in modern bivalved mollusc shells, *Geochimica et Cosmochimica Acta*, **142**, 400–410, <http://doi.org/10.1016/j.gca.2014.07.017>

Price, N. J. 1966. *Fault and joint development in brittle and semi-brittle rock*, Pergamon Press, 176pp

Quirk, D. G. 1993. Origin of the Peak District Orefield, *Bulletin of the Peak District Mines Historical Society*, **12**, 4–15.

Rutter, E. H., McKernan, R. *et al.* 2013. Permeability of stress-sensitive formations: its importance for shale gas reservoir simulation and evaluation. [http://www.petro-online.com/articles/measurement-and-testing/14/e.h.\\_rutter\\_r.mckernan\\_j.mecklenburgh\\_s.e.\\_may/permeability\\_of\\_stress-sensitive\\_formations\\_its\\_importance\\_for\\_shale\\_gas\\_reservoir\\_simulation\\_and\\_evaluation\\_/1476/](http://www.petro-online.com/articles/measurement-and-testing/14/e.h._rutter_r.mckernan_j.mecklenburgh_s.e._may/permeability_of_stress-sensitive_formations_its_importance_for_shale_gas_reservoir_simulation_and_evaluation_/1476/)

Sangster, D. F., Nowlan, G. S. & McCracken, A.D. 1994. Thermal comparison of Mississippi Valley-Type lead-zinc deposits and their host rocks using fluid inclusion and conodont color alteration index data, *Economic Geology*, **89**, 493–514

Santrock, J., Studely, S.A., & Hayes, J.M. 1985. Isotopic analyses based on the mass spectrum of carbon dioxide, *Analytical Chemistry*, **57**, 1444-1448

Schauer, A. J., Kelson, J., Saenger, C., & Huntington, K. W. (2016). Choice of 17O correction affects clumped isotope ( $\Delta 47$ ) values of CO<sub>2</sub> measured with mass spectrometry. ... In *Mass Spectrometry*, 30(24), 2607–2616. <http://doi.org/10.1002/rcm.7743>

Sheppard, S. M. F. 1986. Characterization and Isotopic Variations in Natural Waters, *Reviews in Mineralogy and Geochemistry*, **16**, 165–184.

Sheppard, S. & Gilg, H. A. 1996. Stable isotope geochemistry of clay minerals, *Clay Minerals*, **31**, 1–24.

Sibson, R. H., Moore, J. M. & Rankin, A. H. 1975. Seismic pumping—a hydrothermal fluid transport mechanism. *Journal of the Geological Society*, **131**, 653–659,  
<http://doi.org/10.1144/gsjgs.131.6.0653>

Sibson, R. H. 1981. Fluid Flow Accompanying Faulting: Field Evidence and Models, *In*: Simpson, D.W. & Richards, P.G. (eds) *Earthquake Prediction*, Maurice Ewing series, American Geophysical Union, **4**, 593-603, <http://doi.org/10.1029/ME004p0593>

Sibson, R. H. 1987. Earthquake rupturing as a mineralizing agent in hydrothermal systems, *Geology*, **15**, 701–704, <http://doi.org/10.1130/0091-7613>

Siman-Tov, S., Affek, H. P., Matthews, A., Aharonov, E., & Reches, Z. (2016). Shear heating and

clumped isotope reordering in carbonate faults. *Earth and Planetary Science Letters*, **445**, 136–145.  
<http://doi.org/10.1016/j.epsl.2016.03.041>

Stolper, D. A., & Eiler, J. M. (2015). The kinetics of solid-state isotope-exchange reactions for clumped isotopes: A study of inorganic calcites and apatites from natural and experimental samples. *American Journal of Science*, **315**(5), 363–411. <http://doi.org/10.2475/05.2015.01>

Swanson, E. M., Wernicke, B. P. *et al.* 2012. Temperatures and fluids on faults based on carbonate clumped-isotope thermometry, *American Journal of Science*, **312**, 1–21,  
<http://doi.org/10.2475/01.2012.01>

Tsuneishi, Y. & Nakamura, K. 1970. Faulting Associated with the Matsushiro Swarm Earthquakes, *Bulletin of the Earthquake Research Institute*, **48**, 29–51

Wacker, U., Fiebig, J. *et al.* 2014. Empirical calibration of the clumped isotope paleothermometer using calcites of various origins, *Geochimica et Cosmochimica Acta*, **141**, 127–144,  
<http://doi.org/10.1016/j.gca.2014.06.004>

Walkden, G. M. & Williams, D. O. 1991. The diagenesis of the late Dinantian Derbyshire-East Midland carbonate shelf, central England, *Sedimentology*, **38**, 643–670.

Wang, Z., Schauble, E. A. & Eiler, J. M. 2004. Equilibrium thermodynamics of multiply substituted isotopologues of molecular gases, *Geochimica et Cosmochimica Acta*, **68**, 4779–4797,  
<http://doi.org/10.1016/j.gca.2004.05.039>

Wilkinson, J. J. Stoffell, B. *et al.* 2009. Anomalously metal-rich fluids form hydrothermal ore deposits. *Science*, **323**, 764–767. <http://doi.org/10.1126/science.1164436>

Wright, V., Woodcock, N. H. & Dickson, J. A. D. 2009. Fissure fills along faults: Variscan examples from Gower, South Wales, *Geological Magazine*, **146**, 890–902,  
<http://doi.org/10.1017/S001675680999001X>

**Fig. 1.** Location and regional geology of the Peak District area of the southern Pennines. **(a)** geographic location; **(b)** Viséan palaeogeography showing the distribution of basement (Wales-Brabant High), platform and basin facies sediments. Major normal growth faults that bound the basins are indicated in red; **(c)** Location of Dirlow Rake [SK148 818] in relation to the platform margin and major mineralized faults and veins indicated in red. The line A - B marks the line of the schematic section shown in Figure 2. The dotted line that runs sub-parallel to the line of section marks the approximate line of the seismic section shown in Figure 2.

**Fig. 2.** **(a)** Section across the northern margin of the Derbyshire Platform (A - B in Figure 1). The section detail is informed by the seismic profile shown in panel **(b)**. The Castleton Fault that forms the southern margin of the Edale Basin is not exposed at the surface but is clear in the seismic profile. Dirlow Rake is a splay of the Castleton Fault. Profile and section are from Andrews (2013).

**Fig. 3.** **(a)** Hand specimen sized piece of DLR7. The vein grew from right to left with dog tooth spar terminations clearly visible on the left hand edge. **(b)** PPL thin section image of DLR7 showing scalenohedral surfaces marked by planar trails with a high inclusion density. **(c)** Under XPL these surfaces are characterised by small, irregular crystals of calcite that have nucleated on crystal surfaces. These crystals have a random orientation at variance with the overall optical continuity of the vein calcite. We interpret the surfaces as representing a hiatus in crystal growth before a new episode of calcite precipitation associated with the influx of a pulse of hydrothermal fluid.

**Fig. 4.**  $\delta^{13}\text{C}$ ,  $\delta^{18}\text{O}$  and  $T(\Delta_{47})$  values plotted for two transects in the growth direction of vein DLR7. **(a)** section DLR7-a, and **(b)** section DLR7-b. The two profiles are displaced laterally and with respect to their zero datum from each other. The grey bars are drawn where there is a marked positive step transition in  $\delta^{18}\text{O}$  accompanied by a drop in precipitation temperature as indicated by  $T(\Delta_{47})$ .

**Fig. 5.** **(a)**  $\delta^{13}\text{C}$  versus  $\delta^{18}\text{O}$ ; **(b)**  $T(\Delta_{47})$  versus  $\delta^{13}\text{C}$ ; **(c)**  $T(\Delta_{47})$  versus  $\delta^{18}\text{O}$  for DLR7-a and DLR7-b. The solid line plotted in (c) represents the calculated trend for the oxygen isotopic composition of calcite precipitated from a 2-component mixed fluid (fluid A:  $T = 100^\circ\text{C}$ ,  $\delta^{18}\text{O} = 4.85\text{‰}_{\text{VSMOW}}$ ; fluid B:  $T = 30^\circ\text{C}$ ,  $\delta^{18}\text{O} = -4.13\text{‰}_{\text{VSMOW}}$ ); **(d)**  $T(\Delta_{47})$  versus fluid  $\delta^{18}\text{O}$ . Representative error ellipses (90% confidence interval) corresponding to the highest and lowest temperature data points are indicated. The calcite  $\delta^{18}\text{O}$  isopleths represent the loci of values in equilibrium with water (x-axis) at temperature (y-axis).

**Fig. 6.** Plot of  $T(\Delta_{47})$  versus fluid- $\delta^{18}\text{O}$  modified after Figure 5(d). The fields of the low temperature meteoric and high temperature basin fluid end-members are indicated. The field of waters that would be in equilibrium with the host Dinantian limestones at temperatures between  $105^\circ$  and  $115^\circ\text{C}$  is calculated using as limits (i) the whole rock  $\delta^{18}\text{O}$  value of  $-6\text{‰}_{\text{VPDB}}$ , and (ii) a suggested value of  $-2.4\text{‰}_{\text{VPDB}}$  for least altered Dinantian marine limestones (Walkden & Williams 1991). The solid line tracks the composition of connate marine waters in isotopic equilibrium with kaolin in shales and assuming a 20% initial porosity and an initial  $\delta^{18}\text{O}$  of the kaolin of  $+20\text{‰}_{\text{VSMOW}}$ .

**Fig. 7.** Plot of  $T(\Delta_{47})$  versus  $\delta^{18}\text{O}$  modified after Figure 5(c). The 2-component mixing trend plots the expected trajectory of calcite  $\delta^{18}\text{O}$  values for mixing of a basin derived fluid with a local meteoric water, as described for Figure 5. The cooling trend represents the evolution of calcite  $\delta^{18}\text{O}$  values for a fluid with an initial temperature of 100°C, and  $\delta^{18}\text{O}$  value of +4.85‰<sub>VSMOW</sub>. The mixing model is clearly a better description of the observed data trends than the model involving the cooling of a high temperature fluid.

**Fig 8.** Schematic of a simple energy balance model to describe the rapid ascent of a high temperature fluid along an idealised planar fault surface. Heat energy used in (i) heating the immediate fault zone, and (ii) due to thermal diffusion perpendicular to the fault surface is balanced by that lost from the rising fluid. The energy balance allows an estimate of the likely range of fluid fluxes necessary to sustain a small temperature drop in the rising fluid.

**Fig 9.** Basin evolution model for the Edale Gulf and adjacent Derbyshire platform. The Visean-Namurian boundary both in the basin and on the platform are indicated. Isotherms are from the estimates of Colman et al. (1989) and Walkden and Williams (1991). The age of the mineralisation based on the range of evidence summarised at the bottom of the diagram is early Permian and towards the end of the late Visean uplift. Fluids originating from the shale units of the Bowland-Hodder group in the basin rise rapidly along the Castleton and associated faults to a depth of approximately 1km where mineralization takes place. The repeated rupture of the shale and subsequent faulting may occur as overpressured cells within sediment units pass through the lithostatic pressure gradient curve during uplift.

**Table 1.** Analytical results

Sample	x (mm)	$\delta^{13}\text{C}$ (VPDB)	$\delta^{18}\text{O}$ (VPDB)	$\Delta_{47}$ (ARF) <sup>†</sup>	$\Delta_{48}$ (LRF) <sup>‡</sup>	T (°C)	$1000\ln\alpha^{\S}$	$\delta^{18}\text{O}_{\text{water}}$ (VSMOW)
DLR7a-a	0	3.45	-9.55	0.541	-0.02	72	19.881	+0.9
DLR7a-b	5	3.52	-9.81	0.506	-0.15	92	16.964	+3.6
DLR7a-c	10	3.30	-8.21	0.597	-0.06	46	24.145	-2.0
DLR7a-d	15	3.46	-8.77	0.580	-0.03	53	22.897	-1.3
DLR7a-e	20	2.71	-9.05	0.547	-0.04	69	20.339	+1.0
DLR7a-f	25	2.52	-9.19	0.545	-0.01	70	22.803	+0.9
DLR7a-f *	25	2.51	-9.07	0.538	-0.08	73	19.646	+1.6
DLR7a-g	30	1.84	-8.08	0.592	-0.03	48	23.756	-1.5
DLR7a-g *	30	1.84	-7.92	0.580	-0.01	53	22.930	-0.5
DLR7a-h	35	3.33	-8.48	0.565	-0.04	60	21.785	+0.1
DLR7a-h *	35	3.35	-8.47	0.518	-0.20	84	18.000	+1.0
DLR7a-i	40	3.12	-8.54	0.575	-0.13	55	22.514	-0.7
DLR7a-i *	40	3.19	-8.57	0.547	-0.14	68	20.376	+1.4
DLR7a-j	45	3.08	-8.51	0.525	-0.12	81	18.540	+3.3
DLR7a-j *	45	3.06	-8.53	0.542	-0.06	71	19.931	+1.9
DLR7a-k	50	3.51	-8.80	0.535	+0.06	75	19.379	+2.2
DLR7a-l	55	3.67	-8.76	0.563	-0.04	61	21.613	0.0
DLR7a-m	60	3.46	-8.86	0.565	-0.07	60	21.752	-0.3
DLR7a-n	65	3.61	-9.35	0.556	-0.09	64	21.057	-0.1
DLR7a-o	70	3.67	-9.48	0.540	0.00	72	19.812	+1.1
DLR7a-p	75	3.47	-9.39	0.536	-0.14	74	19.458	+1.5
DLR7a-q	80	2.34	-9.42	0.521	-0.13	83	18.217	+2.7
DLR7b-a	0	3.66	-8.92	0.555	-0.05	64	21.008	+0.4
DLR7b-b	5	3.49	-9.14	0.577	+0.03	54	22.641	-1.4
DLR7b-c	10	1.66	-7.34	0.635	0.00	31	26.915	-3.9
DLR7b-d	15	3.19	-9.08	0.522	-0.19	82	18.311	+3.0
DLR7b-e	20	3.50	-9.42	0.493	-0.24	100	15.880	+5.1
DLR7b-f	25	3.60	-9.48	0.510	-0.08	90	17.288	+3.6
DLR7b-g	30	3.51	-9.76	0.525	-0.14	81	18.541	+2.0
DLR7b-h	35	3.65	-9.64	0.543	-0.07	71	19.984	+0.7
DLR7b-i	40	3.67	-9.78	0.501	-0.21	95	16.583	+4.0
DLR7b-j	45	3.65	-9.71	0.563	-0.02	61	21.560	-0.9
DLR7b-k	50	3.31	-9.73	0.540	-0.05	72	19.804	+0.8
DLR7b-l	55	3.09	-8.76	0.584	-0.27	51	23.210	-1.6
DLR7b-m	60	3.44	-9.60	0.496	-0.18	99	16.091	+4.7
DLR7b-n	65	3.34	-8.86	0.589	-0.16	49	23.557	-2.1
DLR7b-o	70	2.93	-9.10	0.546	-0.06	69	20.273	+1.0
DLR7b-p	75	3.47	-9.80	0.520	-0.13	84	18.121	+2.4
DLR7b-q	80	3.57	-9.87	0.535	-0.18	75	19.347	+1.1
DLR7b-r	85	3.40	-8.68	0.585	-0.10	51	23.252	-1.6

\* replicate analyses

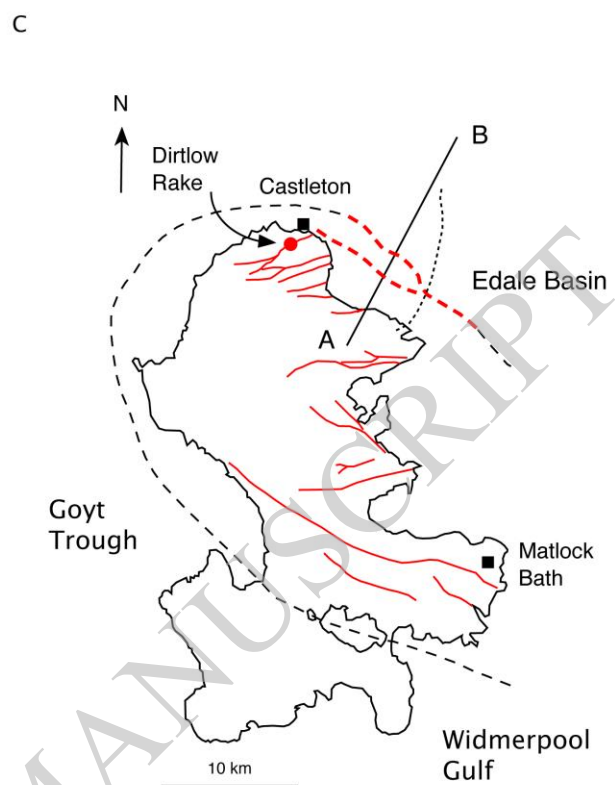
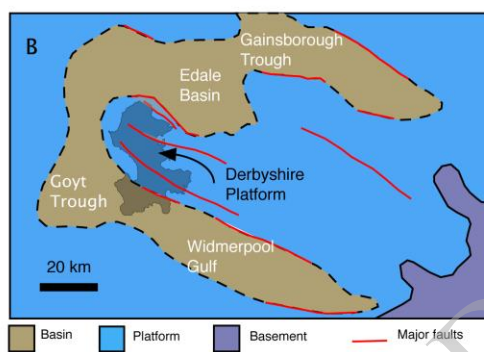
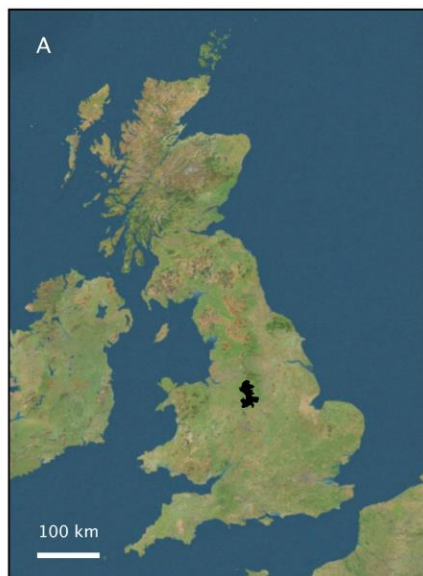
<sup>†</sup> ARF = Absolute Reference Frame (Dennis *et al.* 2011). Measurement precision = +/-0.014%

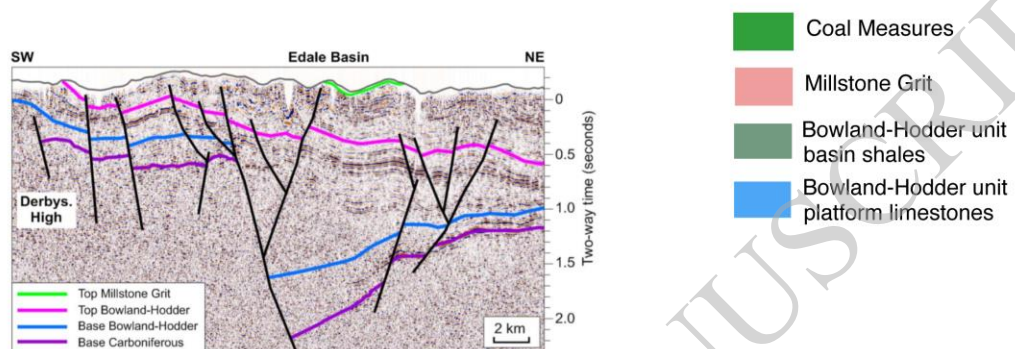
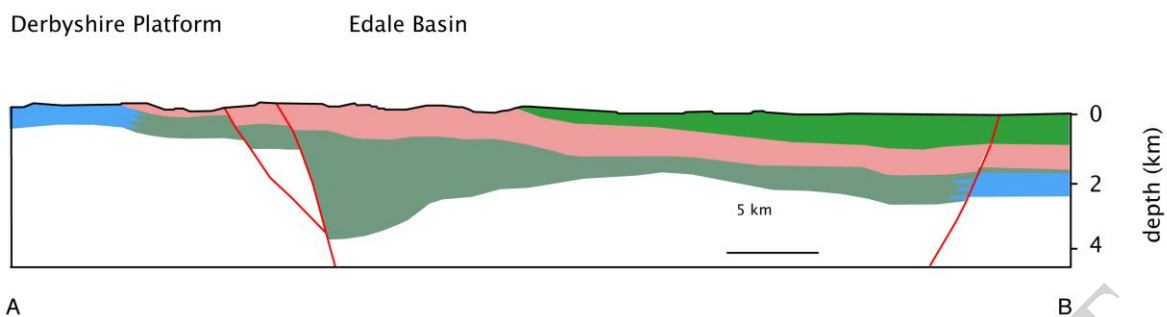
<sup>‡</sup> LRF = Local Reference Frame i.e. measured wrt the mass spectrometer working reference gas

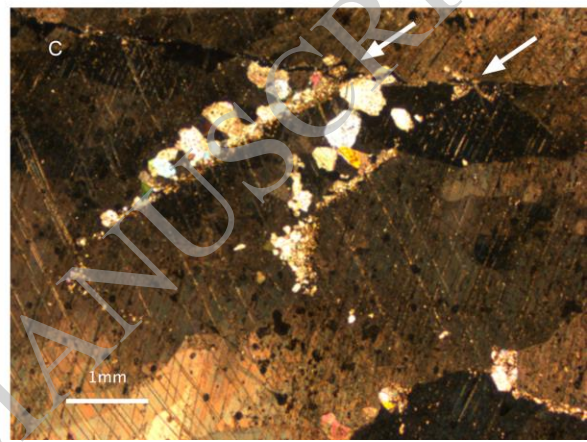
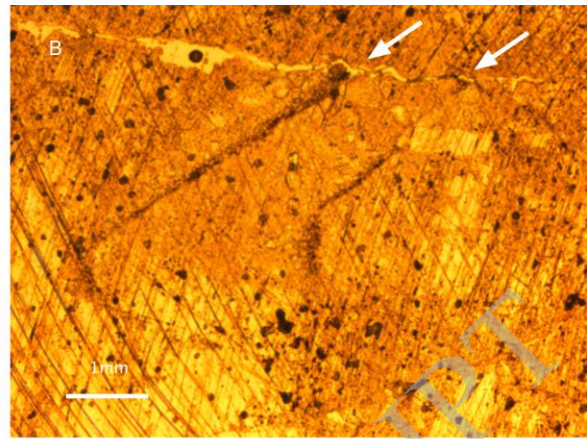
<sup>§</sup> Determined using the estimated  $T(\Delta_{47})$ ,  $\delta^{18}\text{O}$  of the calcite and the Kim and O'Neil (1997) calibration of the calcite-water equilibrium fractionation factor,  $\alpha$

**Table 2.** Calculated fluid volumes and fluxes based on the energy balance model, eqn. 10 and Figure 8

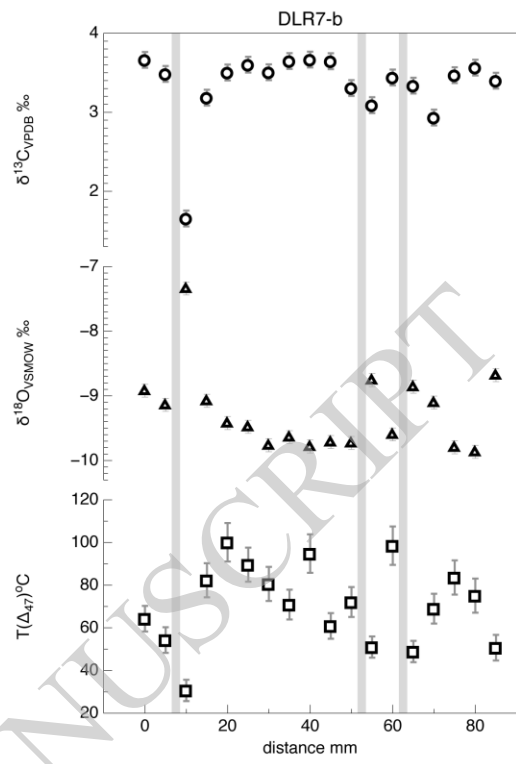
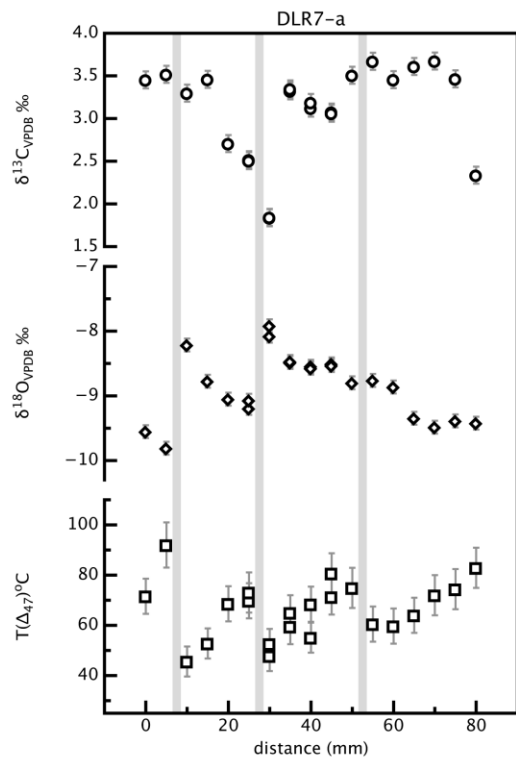
$\Delta\Phi$ (%)	V (m <sup>3</sup> )	h = 1m		h = 10m	
		t (y)	J (m <sup>2</sup> hr <sup>-1</sup> )	t (y)	J (m <sup>2</sup> hr <sup>-1</sup> )
0.1	$8 \times 10^4$	68	$1.36 \times 10^{-1}$	46	$1.98 \times 10^{-1}$
1.0	$8 \times 10^5$	6912	$1.32 \times 10^{-2}$	6678	$1.37 \times 10^{-2}$
10.0	$8 \times 10^6$	694000	$1.30 \times 10^{-3}$	691000	$1.32 \times 10^{-3}$



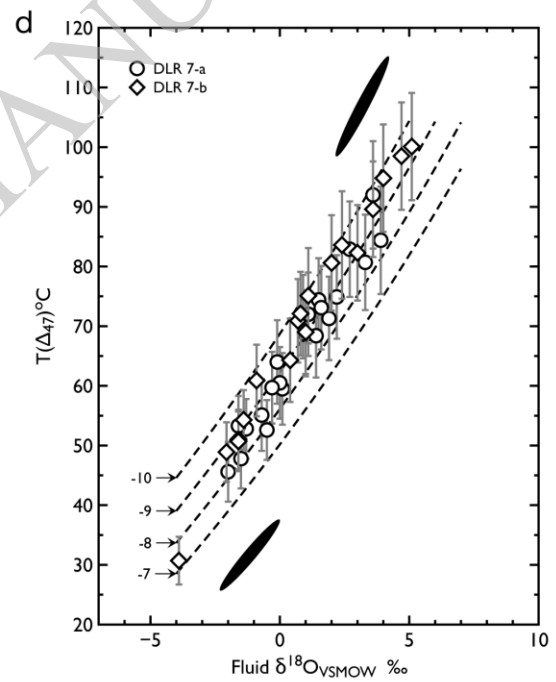
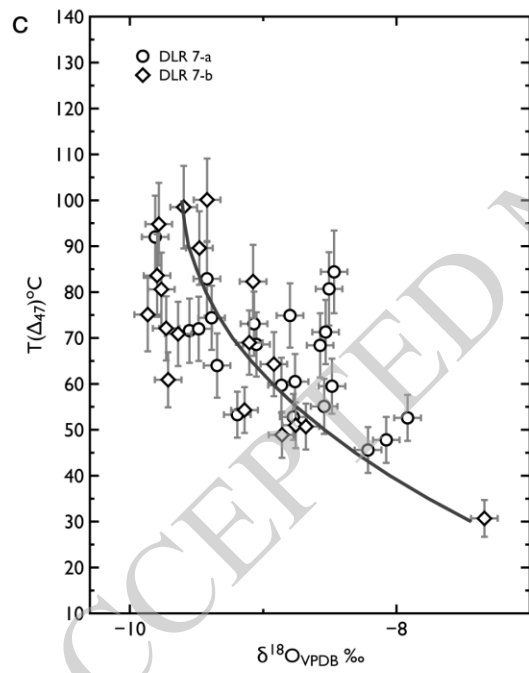
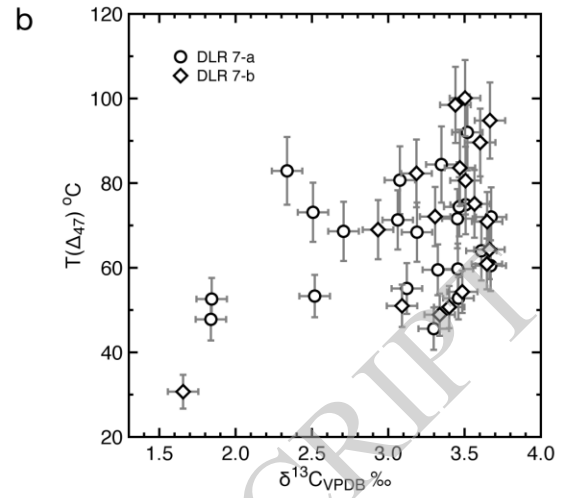
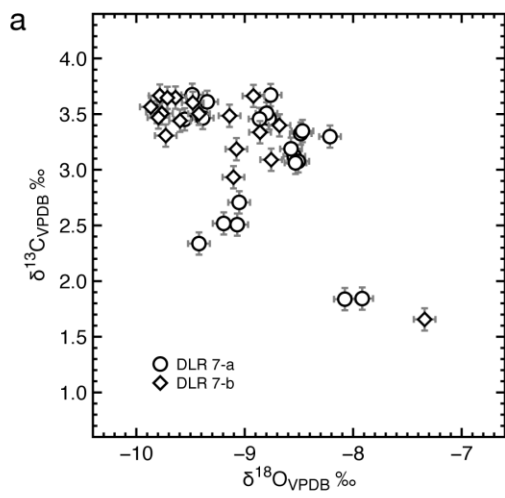


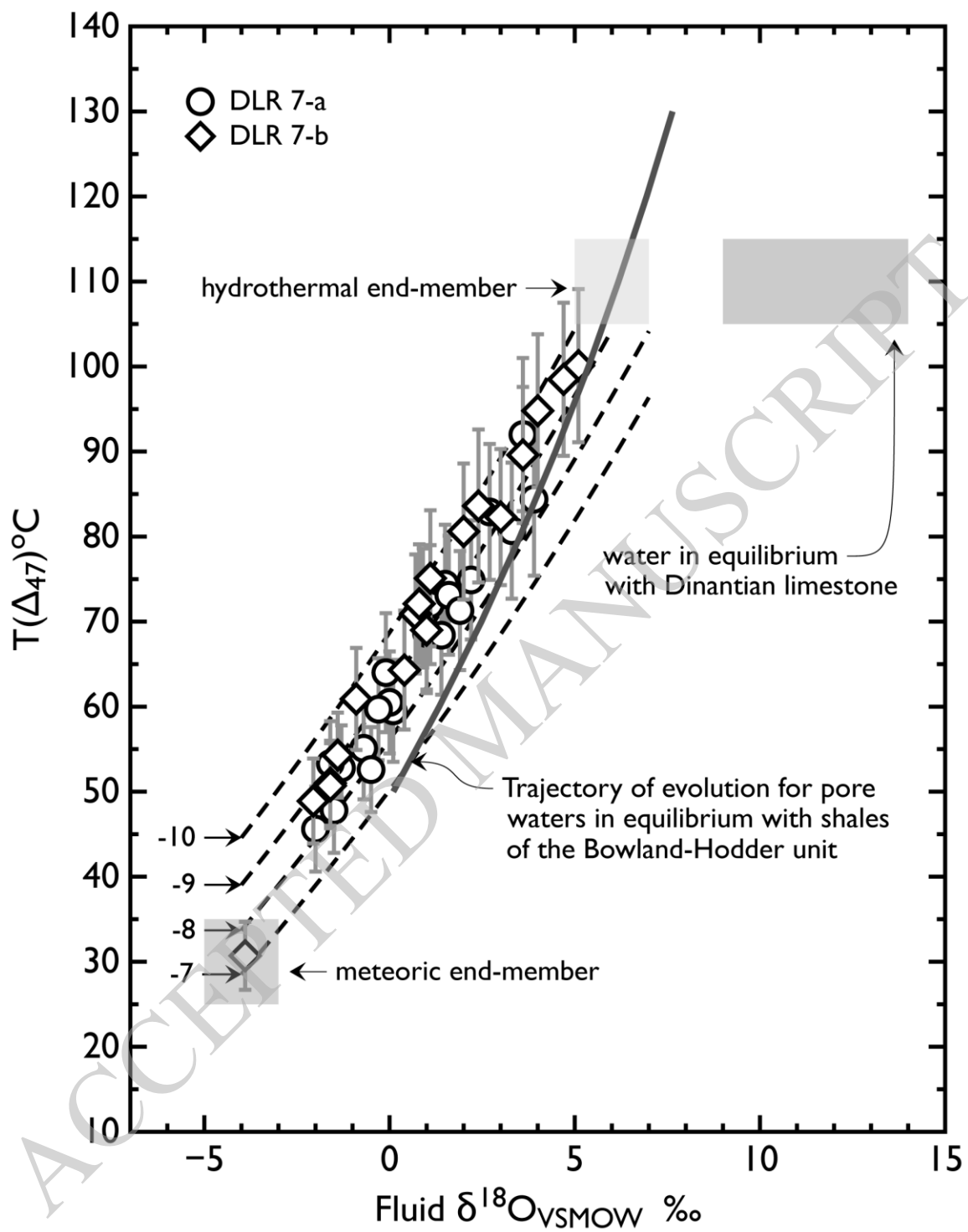


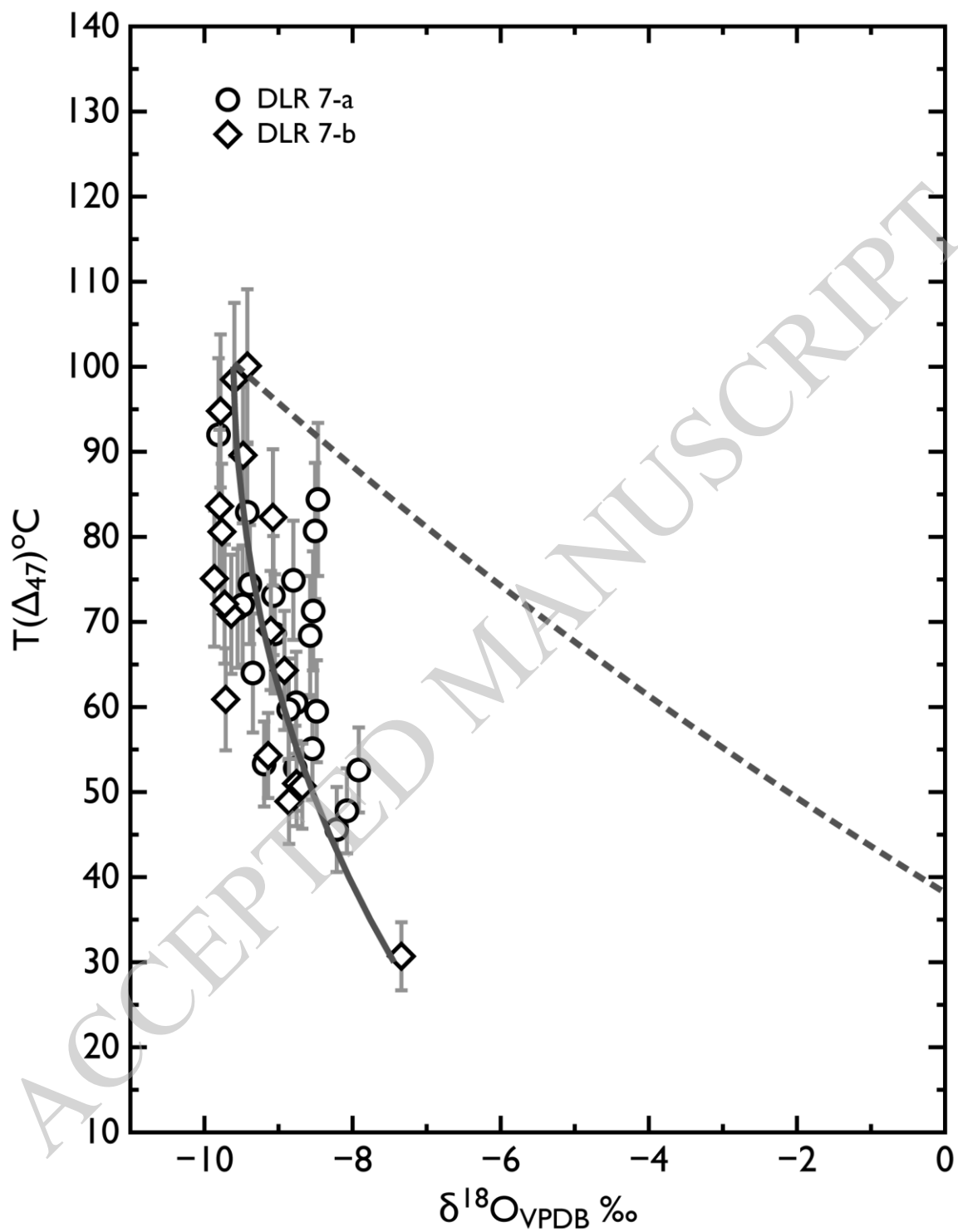
ACCEPTED MANUSCRIPT

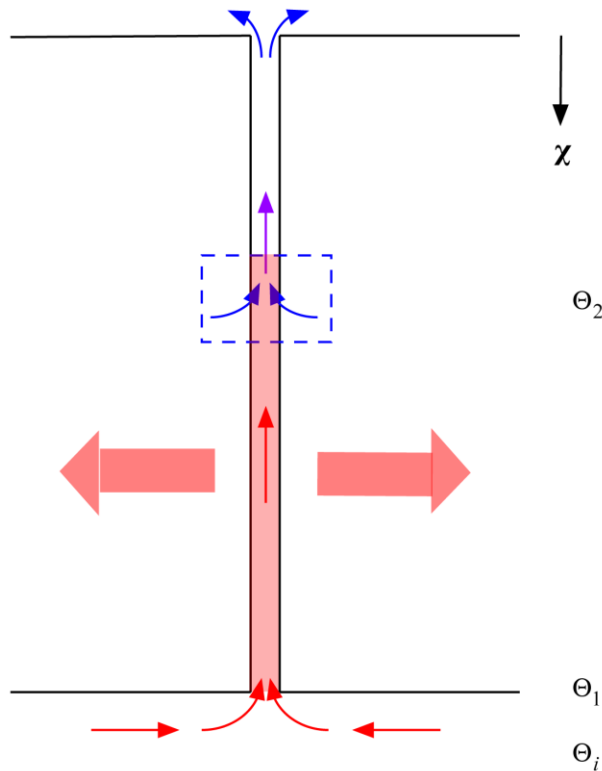


ACCEPTED MANUSCRIPT









Heat required to raise  
fault T to  $\Theta_1$

$$\Delta H_a = (x_1 - x_2) \cdot h \cdot \left( \frac{\Theta_1 - \Theta_2}{2} \right) \cdot C_p^r \cdot \rho_r$$

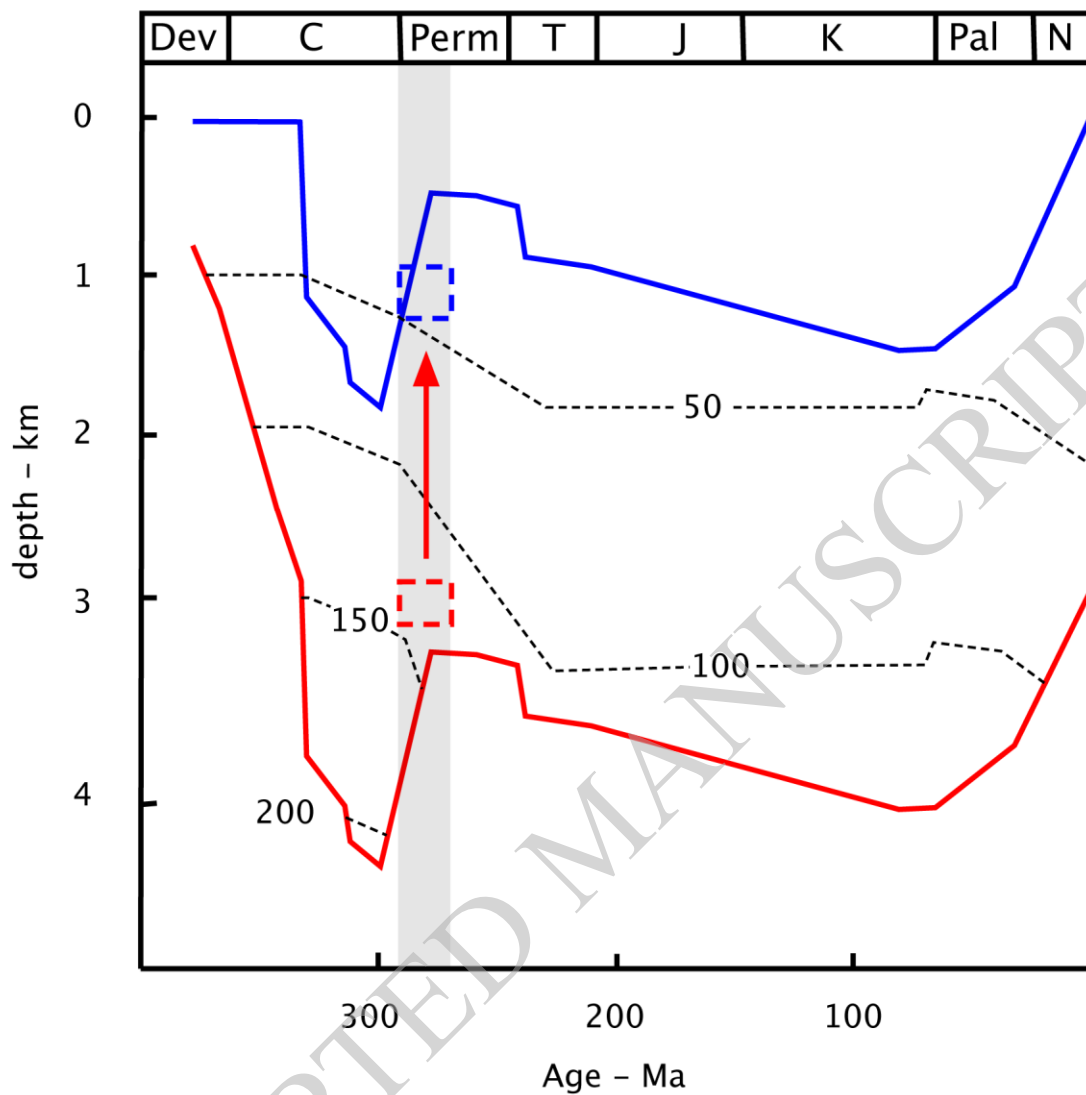
Heat lost to thermal diffusion  
(Crank, 1975 - eqn 3.15)

$$\Delta H_b = (x_1 - x_2) \cdot (\Theta_1 - \Theta_2) \cdot \left( \frac{kt}{\pi} \right)^{0.5} \cdot C_p^r \cdot \rho_r$$

Energy balance

$$(\Theta_i - \Theta_1) \cdot V \cdot C_p^w \cdot \rho_w = \Delta H_a + \Delta H_b$$

ACCEPTED MANUSCRIPT



- Mineralisation
- 4-He residence time
- Oil generation window
- Gas generation window
- Variscan inversion
- Early meteoric diagenesis
- 270Ma K-Ar date